

A bootstrap procedure for parameter estimation in
the spatio-temporal epidemic-type aftershock
sequence model

Renjie Peng

Department of Mathematics and Statistics

McGill University, Montréal

DECEMBER, 2022

A thesis submitted to McGill University in partial fulfillment
of the requirements of the degree of

Master of Science

© Renjie Peng, 2022

Acknowledgements

This thesis was conducted under the supervision of Professors Christian Genest and Pierre Dutilleul, to whom I express my sincere gratitude. Their help throughout my research and the writing of my thesis, as well as their kind sharing of their time and knowledge, is greatly appreciated. Their encouragement and support not only inspired me to complete this thesis but also strengthened my faith to continue my academic journey. Their enthusiasm for research and life has also positively influenced my life. When I face difficulties for the rest of my life, the phrase "never give up" will always inspire me.

Second, I greatly appreciate Professor Jiancang Zhuang from the Institute of Statistical Mathematics, Japan, and Professor David A. Stephens from McGill University. I am grateful to Professor Zhuang for generously providing his paper's original codes, allowing me to jump-start my research. I am also thankful to Professor Stephens for allowing me to access Compute Canada, which saved me a lot of time.

Third, I want to extend my deep gratitude to McGill University and the people here, particularly Professors Abbas Khalili, Johanna G. Nešlehová, Masoud Asgharian, David Wolfson, Russell Steele, and Linan Chen. Their excellent lectures and the rewarding experience of my graduate studies at McGill University have equipped me with a solid foundation and instilled in me the energy to pursue my academic dream.

Last but not least, I gratefully acknowledge funding in support of this work provided by the Department of Mathematics and Statistics at McGill University, the Natural Sciences and Engineering Research Council of Canada, the Canada Research Chair in Dependence Modeling, and the Trottier Institute for Science and Public Policy.

Abstract

The 2-D spatio-temporal epidemic-type aftershock sequence (ETAS) model is used to decluster earthquake data catalogs as well as to make short-term forecasts of future seismic events. Usually, the calculation of standard errors of the ETAS model parameter estimates is based on the Hessian matrix derived from the log-likelihood function of the associated ETAS model. However, when an ETAS model is fitted to a local data set, the standard errors based on the Hessian matrix may be inaccurate. In this thesis, the ETAS model was fitted to a coastal earthquake data set for British Columbia. A parametric bootstrap procedure was used to assess the accuracy of the estimates' asymptotic standard errors. It was found that the finite-sample distribution of some of these parameter estimators is not Gaussian and that, as a result, the asymptotic standard errors are not reliable. To show that the bootstrap procedure provides a reliable standard error estimate and confidence interval for each model parameter, a Monte Carlo simulation study was performed using known parameter values in the same range as those corresponding to the real data. Edge effects were found to be important both in time and space, both in the bootstrap method and in the simulation study. After modifying the procedure to take these effects into account, a retrospective forecasting experiment was carried out to predict earthquakes west of Vancouver Island before and after the magnitude 6.1 earthquake that occurred on October 22, 2018. Finally, the asymptotic and bootstrap standard errors were further compared, along with the asymptotic and bootstrap confidence intervals obtained from empirical quantiles, by applying repeatedly the bootstrap procedure with 1000 bootstrap simulations for 40 Monte Carlo simulations.

Résumé

La version spatio-temporelle 2-D du modèle ETAS des répliques épidémiques est un outil de désagrégation des catalogues de données sur les séismes et de prévision des répliques à court terme. Le calcul de l'écart-type des estimations des paramètres de ce modèle est généralement fondé sur la matrice hessienne déduite de la log-vraisemblance. Lorsqu'un modèle ETAS est ajusté à des données locales, les écarts-types ainsi obtenus peuvent parfois s'avérer imprécis. Dans ce mémoire, le modèle ETAS a été ajusté à des données sismiques au large de la Colombie-Britannique. Une procédure de bootstrap paramétrique a été utilisée pour évaluer l'exactitude de l'écart-type des estimations. Il apparaît que la loi à taille finie de ces estimations n'est pas gaussienne et que, par conséquent, les écarts-types asymptotiques ne sont pas fiables. Pour montrer que la procédure bootstrap fournit des estimations d'écart-type et des intervalles de confiance fiables pour tous les paramètres du modèle, une étude de Monte-Carlo a été réalisée pour des valeurs de paramètres connues semblables à celles correspondant aux données réelles. Les effets de bord se sont avérés importants dans le temps et dans l'espace, tant pour la méthode bootstrap que dans l'étude de simulation. Après avoir modifié la procédure pour tenir compte de ces effets, une expérience de prévision rétrospective a été réalisée afin de prédire les répliques au large de l'île de Vancouver avant et après le séisme de magnitude 6.1 survenu le 22 octobre 2018. Finalement, les écarts-types asymptotique et bootstrap ont aussi été comparés, de même que les intervalles de confiance asymptotique et bootstrap (déduit des quantiles empiriques dans le second cas), en appliquant de façon répétitive la procédure bootstrap 1000 fois pour 40 simulations de type Monte-Carlo.

Author contributions

Except as noted below, everything in this dissertation is my original work. None of the content was produced in conjunction with anyone else.

The original problem description was proposed by Professors Christian Genest and Pierre Dutilleul. The data used in this study were derived from the National Earthquake Database, which is available at <http://earthquakescanada.nrcan.gc.ca/stndon/NEDB-BNDS/bulletin-en.php>. I proposed a bootstrap procedure and completed the implementation and analysis under the guidance of my supervisors, who helped me in choosing the techniques and refining my study. I was also responsible for the first draft of the thesis, which contains three chapters. In particular, Chapter 2 is a manuscript. The presentation, contents, and formulation of this thesis benefited from the comments of Professors Christian Genest and Pierre Dutilleul.

Table of Contents

Acknowledgements	i
Abstract	ii
Résumé	iii
List of Figures	ix
List of Tables	xii
1 Introduction	1
2 Manuscript	4
2.1 Introduction	4
2.2 Self-exciting spatio-temporal point processes	6
2.2.1 Temporal form	6
2.2.2 Spatio-temporal form	7
2.2.3 Marked self-exciting point processes	8
2.3 The ETAS model	9
2.3.1 2-D spatio-temporal ETAS model	9
2.3.2 ETAS model terminology	12
2.3.3 Stochastic declustering	13
2.3.4 Parameter estimation and model fitting	14
2.4 Earthquake data catalog	17
2.4.1 Completeness of the earthquake data catalog	18
2.4.2 Stationarity in time	20

2.4.3	Summary	21
2.5	The ETAS model fitting procedure	22
2.6	A bootstrap procedure to build confidence intervals for the ETAS model parameters	24
2.6.1	Bootstrap simulation procedure	25
2.6.2	Analysis based on the parametric bootstrap simulation	27
2.7	A Monte Carlo simulation study	35
2.7.1	Methodology	35
2.7.2	Results	36
2.8	Forecasting	37
2.8.1	Simulation-based forecasting procedure	37
2.8.2	A retrospective forecasting experiment	39
2.9	Discussion: Use of the bootstrap procedure for Monte Carlo simulations . .	44
3	Conclusion	47
	References	50
A		53
B		67
C		70

List of Figures

2.1	A geographic map of the region of interest in this study.	19
2.2	Plots of $\log_{10}(N_{\text{mag}})$ versus mag (magnitude) by increments of 0.1 from 0, 2.5, 3.5, and 4 in panels (a), (b), (c), and (d), respectively.	20
2.3	Plot of the number of earthquakes in the catalog before time t versus time t . The x -axis represents the lag (day) from the start time of the earthquake catalog, 2000/01/01 00:00:00. The left red dashed vertical line marks the 2008/04/27 00:00:00, and the right red dashed vertical line marks the end of the study period 2018/04/27 00:00:00.	21
2.4	Map of the earthquakes used in the ETAS model fitting. The red frame delineates the study space window. The blue circles represent the target events while the grey circles represent the complementary events. The size of each circle is proportional to the magnitude of the corresponding earthquake.	22
2.5	Boxplots derived from 1000 estimates (including the three extremely large outliers) obtained for seven of the ETAS model parameters by bootstrap simulation. In each boxplot, the red line represents the putative value of the corresponding parameter, the blue line marks the mean of the 1000 estimates, and the two green lines are the 2.5% and 97.5% empirical quantiles of the distribution of of the estimates, respectively.	28
2.6	Space-time plots of the latitudes (left) and longitudes (right) against the times of occurrence of earthquakes in the simulated data set 573.	30

2.7	Space-time plots of the latitudes (left) and longitudes (right) against the times of occurrence of earthquakes in the simulated data set 672.	30
2.8	Space-time plots of the latitudes (left) and longitudes (right) against the times of occurrence of earthquakes in the simulated data set 823.	30
2.9	Space-time plots of the latitudes (left) and longitudes (right) against the times of occurrence of earthquakes in the real earthquake data catalog. . . .	31
2.10	Boxplots derived from 1000 estimates (excluding the three extremely large outliers) obtained for seven of the ETAS model parameters by bootstrap simulation. In each boxplot, the red line represents the putative value of the corresponding parameter, the blue line marks the mean of the 1000 estimates, and the two green lines are the 2.5% and 97.5% empirical quantiles of the distribution of of the estimates, respectively.	32
2.11	Boxplots of asymptotic standard errors of the estimates for each parameter from the 1000 simulated data sets.	33
2.12	Map of earthquakes in the earthquake data catalog of interest. The blue circles represent the events in the space-time window built by space window (longitude: 126.75°W–130.5°W, latitude: 48.25°N–49.75°N) and time interval ([2008/04/27 00:00:00, 2018/11/21 00:00:00]), while the grey circles indicate the complementary events in the catalog. The size of each circle is proportional to the magnitude of the corresponding earthquake. . .	40
2.13	Left: Plot of $\log_{10}(N_{\text{mag}})$ versus mag (magnitude) by increments of 0.1 from 3.5. Right: Plot of N_t , the number of earthquakes (magnitude ≥ 3.5) in the catalog before time t (day), versus time t (day). The x -axis represents the lag (day) from the start time of the studied earthquake data catalog, 2000/01/01 00:00:00. The left red dashed vertical line indicates 2008/04/27 00:00:00, and the right red dashed vertical line, 2018/11/21 00:00:00, which is the last day in the earthquake data catalog.	41

- 2.14 Plot against time (half-day) of the estimated half-day number of earthquakes (circles in black) in the study space window (longitude: 126.75°W–130.5°W, latitude: 48.25°N–49.75°N) during the time window of interest 2018/10/21 00:00:00 to 2018/11/21 00:00:00. The hexagrams indicate observed numbers of earthquakes in the corresponding half days. The lower and upper green dashed lines represent the 5% and 95% empirical quantiles of the distribution of numbers of simulated earthquakes, respectively. Integer $j \in \{1, \dots, 62\}$ on the x -axis indicates that the forecast is for the j th half day after 2018/10/21 00:00:00. 42
- 2.15 Examples of mapping the estimated intensity function (unit: events/(half-day \times deg²)) over the corresponding time intervals in the study space window to predict the location (epicenter) of earthquakes. In some panels, green circles point to the locations of earthquakes (mag ≥ 3.5) observed. The three red circles in the left graph on the second row indicate the three large earthquakes (mag ≥ 6.0). 44

List of Tables

2.1	Estimates and corresponding asymptotic standard errors (SE) of the ETAS model parameters, obtained with the classical fitting procedure for the earthquake data catalog used as an example.	23
2.2	Three data sets with extremely large outliers obtained in bootstrap simulation.	29
2.3	Observed statistic values and probabilities of significance of the Shapiro–Wilk test	31
2.4	The standard deviation (std) of the asymptotic standard errors calculated for the 1000 simulated data sets.	33
2.5	The estimate, the asymptotic standard error (SE), the bootstrap standard error (bootstrap SE), and the 95% bootstrap confidence interval for seven parameters of the ETAS model.	34
2.6	Three earthquakes with magnitude above 6 on the same date.	40
2.7	Ratios of the mean length of 95% asymptotic confidence intervals (Table C.3) against the mean length of 95% bootstrap confidence intervals (Table C.4) for each of the seven ETAS model parameters studied.	45
A.1	Case 1	53
A.2	Case 2	54
A.3	Case 3	54
A.4	Case 4	55
A.5	Case 5	55

A.6 Case 6	56
A.7 Case 7	56
A.8 Case 8	57
A.9 Case 9	57
A.10 Case 10	58
A.11 Case 11	58
A.12 Case 12	59
A.13 Case 13	59
A.14 Case 14	60
A.15 Case 15	60
A.16 Case 16	61
A.17 Case 17	61
A.18 Case 18	62
A.19 Case 19	62
A.20 Case 20	63
A.21 Case 21	63
A.22 Case 22	64
A.23 Case 23	64
A.24 Case 24	65
A.25 Case 25	65
A.26 Case 26	66
A.27 Case 27	66
 B.1 Estimates of the ETAS model parameters, and the corresponding end of the study time interval.	 67

C.1	Asymptotic standard errors for the estimators of seven parameters of the ETAS model obtained with 40 Monte Carlo simulations using the parameter values reported in Table 2.1 as targets, and their mean value for each parameter.	70
C.2	Bootstrap standard errors for the estimators of seven parameters of the ETAS model obtained with 1000 bootstrap simulations for each of the 40 Monte Carlo simulations in Table C.1, and their mean value for each parameter.	72
C.3	Length of the 95% asymptotic confidence intervals for seven parameters of the ETAS model, obtained with 40 Monte Carlo simulations (i.e., the same 40 Monte Carlo simulations as for Table C.1), and the mean length of these intervals for each parameter.	73
C.4	Length of the 95% bootstrap confidence intervals (derived from the 2.5% and 97.5% empirical quantiles) for seven parameters of the ETAS model, obtained for the 40 Monte Carlo simulations, and the mean length of these intervals for each parameter.	75

Chapter 1

Introduction

Earthquakes are one of the most destructive natural causes of danger ([Oluwafemi et al., 2018](#)). Due to the potential impact of earthquakes on human life, property and even the economy of a country, the global occurrence of earthquakes is a major concern. Thus, it is crucial to develop models to study the occurrence time and location of earthquakes and assess their frequency accurately.

Space-time models for the time of earthquakes and location of their epicenters were developed for analyzing historical data. [Hawkes \(1971\)](#) introduced the self-exciting point process and first applied it to earthquake data in [Hawkes and Adamopoulos \(1973\)](#). Thereafter, [Ogata \(1988\)](#) proposed the ETAS model and examined its likelihood. [Ogata \(1998\)](#) expanded the ETAS model to include both spatial and temporal components, which was later found to be a powerful tool in short-term forecasting of aftershocks ([Zhuang, 2011](#)). In this thesis, the 2-D spatio-temporal ETAS model will be studied.

Earthquakes usually appear to be clustered not only in time but also in space. [Zhuang et al. \(2002\)](#) noted that classifying earthquakes as background events or cluster members is important for forecasting the location of large earthquakes. There are different ways of removing the aftershocks from a cluster of earthquakes. In some methods, a space-time window centered at the large earthquake is drawn and the small earthquakes inside are deleted; see, e.g., [Utsu \(1970\)](#) or [Gardner and Knopoff \(1974\)](#). Instead of imposing a

window, link methods based on the spatial distance and time lag between earthquakes were developed to study association among earthquakes; see [Reasenbergs \(1985\)](#) or [Davis and Frohlich \(1991\)](#), among others.

The strategies mentioned above require that researchers call on their experience to decide on some parameter values in relation to the size of the window or critical values for the spatial distance and time lag, and the optimum choice is hard to make. Instead, [Zhuang et al. \(2002\)](#) proposed a stochastic declustering method, in which the ETAS model is used to overcome these issues. In this thesis, the method of [Zhuang et al. \(2002\)](#) is used to decluster an earthquakes catalog; it will be introduced in detail in Subsection 2.3.3.

The parameters of the ETAS model have a physical interpretation. When the ETAS model is fitted to different local data sets, the differences in the model parameter estimates reflect the different focal processes that generate earthquakes and the various local stress conditions in these places ([Kagan et al., 2010](#)). The standard errors of the estimates are critical in judging whether discrepancies in parameter estimates between areas are significant or not. [Wang et al. \(2010\)](#) stated that when the observable space-time window is narrow, the asymptotic standard errors of the ETAS model parameter estimates based on the Hessian matrix are often inaccurate. [Wang et al. \(2010\)](#) used a simulation method to study the effects of errors in recording the magnitude of earthquakes and the finite size of the time window on the asymptotic standard errors of parameter estimates of the 2-D spatio-temporal ETAS model, which is parameterized differently from the one studied in this thesis. However, these authors did not provide a way to verify the performance of the ETAS model parameter estimates when the corresponding asymptotic standard errors are unreliable.

In this thesis, a new procedure using simulation is developed to study the finite-sample properties of the estimators of the ETAS model parameters and provide an alternative confidence interval for each parameter when the asymptotic standard errors based on the Hessian matrix are deemed to be unreliable. More specifically, the ETAS model is fitted to a coastal earthquake data set for British Columbia, Canada, and the estimates of

model parameters are recorded. These estimates are set as putative values of the corresponding parameters in the ETAS model when the parametric bootstrap (Efron, 1979) is used to simulate the data repeatedly. Estimates of the ETAS model parameters from the simulated data sets are used to approximate the finite-sample distribution of the corresponding parameter estimators. The Shapiro–Wilk test (Shapiro and Wilk, 1965) is used to show that the finite-sample distribution of some parameter estimators is not Gaussian and that, as a result, the corresponding asymptotic standard errors are not reliable. A bootstrap procedure provides a solution to this issue. Then, a Monte Carlo simulation analysis is performed using known parameter values in the same range as those corresponding to the actual data, to verify the performance of estimation and the confidence intervals built with the bootstrap procedure.

Care also needs to be taken to minimize the edge effects when analyzing earthquake data with the 2-D spatio-temporal ETAS model. Because the earthquake data catalog is about a collection of events from a given region and a specified time period, the edge effects cannot be ignored (Zhuang et al., 2004). Otherwise, a bias may be introduced in the parameter estimates of the ETAS model. In particular, missed events in the past history or around the specified regions may induce a downward bias in the number of triggered events when the bootstrap or Monte Carlo simulation is applied.

The rest of this thesis is structured as follows. Chapter 2, which forms the main body of this thesis, consists of a manuscript that describes how the new bootstrap procedure that is proposed can be used to study the finite-sample properties of the ETAS model parameter estimates and to assess the accuracy of their asymptotic standard errors computed from the Hessian matrix. It is also shown therein how a reliable confidence interval for each model parameter can be built, and why the new confidence intervals based on the bootstrap procedure are reliable. At the end of Chapter 2, a retrospective forecasting experiment is carried out to show how the ETAS model can be applied to make an accurate earthquake forecast. Various ways in which this work could be extended are briefly described in Chapter 3, which serves as the Conclusion.

Chapter 2

Manuscript

2.1 Introduction

The 2-D ETAS model is a well-developed instance of a self-exciting spatio-temporal point process that is broadly used to decluster earthquake data catalogs and, to a lower degree, make short-term forecasts of the occurrence time of aftershocks and the location of their epicenter. The temporal version of the ETAS model was proposed by [Ogata \(1988\)](#) and was expanded to a spatio-temporal version by the same author 10 years later ([Ogata, 1998](#)). Based on the 2-D spatio-temporal ETAS model, [Zhuang et al. \(2002\)](#) proposed a stochastic declustering method to identify main shocks and aftershocks in earthquake data catalogs. Thereafter, [Zhuang \(2011\)](#) described how the ETAS model can be used to forecast short-term aftershocks based on simulations.

[Kagan et al. \(2010\)](#) stated that the parameters of the ETAS model have a physical interpretation. When the ETAS model is fitted to different local data catalogs, differences in the model parameter estimates imply that different focal processes generated earthquakes and various local stress conditions. It is thus important to study the accuracy of the parameter estimates and the reliability of the corresponding standard errors.

The parameters of the ETAS model are usually estimated by the method of maximum likelihood. The log-likelihood function of the spatio-temporal ETAS model was intro-

duced by [Ogata \(1998\)](#), and the corresponding standard errors are calculated based on the Hessian matrix derived from this log-likelihood function. [Rathbun \(1996\)](#) stated that the maximum likelihood estimators for spatio-temporal self-exciting point processes are consistent and asymptotically normally distributed as the length of the time span T tends to infinity. However, the time span in local data sets is generally short and limited, and [Wang et al. \(2010\)](#) noted that when the observation space-time window is narrow, the asymptotic standard errors associated with the ETAS model parameter estimates based on the Hessian matrix are often inaccurate.

Therefore, a newly developed bootstrap procedure is presented in this thesis to study the finite-sample properties of the estimators of the ETAS model parameters and provide alternative confidence intervals for parameters when the asymptotic standard errors associated with estimates based on the Hessian matrix are deemed to be unreliable. The proposed procedure is applied to an earthquake data catalog, which contains records on earthquakes in the space frame from 126.25°W to 131°W longitude and from 48°N and 50°N latitude, over the time span from 2000-01-01 00:00:00 to 2019-12-31 23:59:59 (UTC).

A short review of the literature on self-exciting spatio-temporal point processes is given in Section 2.2. The specific 2-D spatio-temporal ETAS model considered here is introduced in Section 2.3, along with the stochastic declustering method based on the ETAS model and the procedure used to fit the ETAS model. The earthquake data catalog of interest in this study is presented in Section 2.4. After fitting the ETAS model, the parameter estimates and the corresponding asymptotic standard errors from the Hessian matrix are reported in Section 2.5. Then, a bootstrap procedure is proposed in Section 2.6 to study the finite-sample properties of the estimators and provide an alternative way of building confidence intervals. In Section 2.7, a Monte Carlo simulation analysis is performed using known parameter values in the same range as those corresponding to the estimates for the real earthquake data catalog to verify the performance of estimation and the confidence intervals built with the bootstrap procedure. A retrospective forecasting

experiment is conducted in Section 2.8. Additional discussion and closing comments are provided in Section 2.9.

2.2 Self-exciting spatio-temporal point processes

Self-exciting spatio-temporal point process models are designed to assess the risk of events, whose occurrence rate depends on location, time, and historical events. This type of model has been widely applied to study earthquakes, the dynamic trend of crime, the spread of infectious diseases, and so on. For the reader's convenience, this section provides a short introduction to this type of model, based on references such as the review papers by [Reinhart \(2018\)](#) and [González et al. \(2016\)](#).

2.2.1 Temporal form

Consider a sequence of events that occurred in the time period $[0, T) \subseteq [0, \infty)$, where 0 represents the beginning of the time period, and the times of occurrence are recorded as $t_1 < \dots < t_n$, where n is the number of events that occurred in the time period $[0, T)$. The set of events that occurred before time t is defined as history H_t . If the occurrence rate of posterior events is assumed to be independent of the historical events H_t , the behavior of the point process for which t_1, \dots, t_n form a partial realization can be characterized by a conditional intensity function as follows

$$\lambda(t|H_t) = \lim_{\Delta t \rightarrow 0} \frac{\mathbb{E}[N\{[t, t + \Delta t)\} | H_t]}{\Delta t},$$

where N is a right-continuous counting measure for the number of events that occurred in the given time interval. If the occurrence rate of events is shown to be affected by the prior events, then a "self-exciting" component should be added to the conditional intensity function.

The temporal self-exciting point process was first proposed by Hawkes (1971). The intensity function is then defined as

$$\lambda(t | H_t) = \nu + \int_0^t g(t-u) dN(u) = \nu + \sum_{i:t_i < t} g(t-t_i).$$

Here, ν is a constant representing the rate at which an event occurs independently and is called the background rate of the events. The triggering function g describes the effect of the historical events on the occurrence rate of the posterior events; it is a function of the time lag between the occurrence time t_i of the i th historical event and time t . Generally, g is a decreasing function, which means that the larger the time lag, the less the effect of the i th event before time t on the occurrence rate at time t . Thus, if the function g decays fast, only the recent events have an effect. Given that the conditional intensity function is nonnegative, the triggering function is always required to be nonnegative.

2.2.2 Spatio-temporal form

If the location of events is important to the occurrence rate of events, the temporal point process can be extended to a spatio-temporal point process. The location of the events is assumed to be described by the longitude and latitude. The rate of events around location $\mathbf{s} = (x, y) \in \mathbf{X} \subseteq [-180^\circ, 180^\circ] \times [-90^\circ, 90^\circ]$ and at time $t \in [0, T] \subseteq [0, \infty)$ can be characterized by the following conditional intensity function

$$\lambda(\mathbf{s}, t | H_t) = \lim_{\Delta s, \Delta t \rightarrow 0} \frac{\mathbb{E}[N\{\mathbf{D}(\mathbf{s}, \Delta s) \times [t, t + \Delta t)\} | H_t]}{|\mathbf{D}(\mathbf{s}, \Delta s)| \Delta t},$$

where $\mathbf{D}(\mathbf{s}, \Delta s)$ is the disk, centered at $\mathbf{s} \in \mathbf{X}$, with radius Δs , and $N\{\mathbf{D}(\mathbf{s}, \Delta s) \times [t, t + \Delta t)\}$ denotes the number of events that occurred in the disk $\mathbf{D}(\mathbf{s}, \Delta s)$ and over the time interval $[t, t + \Delta t)$.

A self-exciting component can be added similarly, and the corresponding conditional intensity function of the point process for which $(\mathbf{s}_1, t_1), \dots, (\mathbf{s}_n, t_n)$ form a partial realiza-

tion can be written as

$$\lambda(\mathbf{s}, t \mid H_t) = \mu(\mathbf{s}) + \sum_{i:t_i < t} g(\mathbf{s} - \mathbf{s}_i, t - t_i),$$

where H_t is the set of events that occurred before time t , the background rate of events is represented by μ , a function of location only, and the triggering function g describes the effect of the i th event before time t on the occurrence rate of events at (\mathbf{s}, t) . For convenience, the triggering function g is often written as the product of a function of location only and a function of time only, i.e., $g(\mathbf{s} - \mathbf{s}_i, t - t_i) = q(\mathbf{s} - \mathbf{s}_i)h(t - t_i)$. Given that the conditional intensity function is nonnegative, the triggering function g is set to be nonnegative as well; for example, it may be a kernel function.

2.2.3 Marked self-exciting point processes

Besides location and time, other features of events can be equally important for certain kinds of events. For earthquakes, in addition to epicenters and times, the magnitude of events is also important, as an earthquake with a larger magnitude is expected to trigger more aftershocks. Moreover, the locations of aftershocks may also be related to the magnitude of the main shock. In such a case, a marked point process can be applied, and the corresponding observations are of the form $\{(\mathbf{s}_i, t_i, m_i), i = 1, 2, \dots\}$, where $\mathbf{s}_i = (x_i, y_i) \in \mathbf{X} \subseteq [-180^\circ, 180^\circ] \times [-90^\circ, 90^\circ]$ and $t_i \in [0, T) \subseteq [0, \infty)$ represent the location and time of the i th event, respectively, and $m_i \in \mathbb{M}$ is the magnitude of the i th event. Here, \mathbb{M} is called the mark space and is a set of earthquake magnitudes of a given type.

The conditional intensity function of a marked spatio-temporal point process can be written as

$$\lambda(\mathbf{s}, t, m \mid H_t) = \lambda_g(\mathbf{s}, t \mid H_t)f(m \mid \mathbf{s}, t, H_t),$$

where λ_g is the conditional intensity function of the "ground process", which is the point process of times and locations of events without their marks, and $f(m | s, t, H_t)$ is the conditional density function of the mark at time t , around location s , and given the history H_t . If the locations and times of the posterior events are affected by the history H_t , a self-exciting component can be similarly added to the conditional intensity function of the ground process λ_g .

In this study, a marked self-exciting spatio-temporal point process will be used to analyze earthquakes, and is introduced in the following section.

2.3 The ETAS model

2.3.1 2-D spatio-temporal ETAS model

Following the first application of a self-exciting point process to an earthquake data catalog by [Hawkes and Adamopoulos \(1973\)](#), [Ogata \(1988\)](#) proposed the simple epidemic-type aftershock sequence (ETAS) model. Later, [Ogata \(1998\)](#) proposed the 2-D spatio-temporal ETAS model, which is now widely used to decluster earthquake catalogs and, to a lesser extent, make short-term forecasts. The papers by [Zhuang et al. \(2002\)](#) and [Zhuang \(2011\)](#) are key references on the subject, and the parametrization of the 2-D spatio-temporal ETAS model proposed in the latter one is adopted here.

An earthquake data catalog includes records on the time, location (longitude, latitude), and magnitude of seismic events over a certain period, in a given region, and above a magnitude threshold m_0 . If we denote the time (decimal day), longitude (degree), latitude (degree), and magnitude of the i th earthquake in the catalog by t_i , x_i , y_i , and m_i for $i \in \{1, \dots, n\}$, the earthquake events reported in the catalog can be considered as a partial realization of a point process on $\mathbb{R}^+ \times \mathbb{R}^2 \times [m_0, \infty)$, where n represents the total number of earthquakes in the catalog ([Ogata, 1998](#)).

In the 2-D spatio-temporal ETAS model, the behavior of the point process for which $\{(t_i, x_i, y_i, m_i), i = 1, \dots, n\}$ is a partial realization is characterized by the conditional in-

tensity function

$$\lambda_{\beta,\theta}(t, x, y, m | H_t) = s_{\beta}(m)\lambda_{\theta}(t, x, y | H_t), \quad (2.1)$$

where β and $\theta = (\nu, A, \alpha, c, p, q, D, \gamma)$ are the model parameters. As explained by [Zhuang et al. \(2002\)](#), the intensity function $\lambda_{\beta,\theta}(t, x, y, m | H_t)$ can be interpreted as the rate at which 'new' earthquakes (after time t) will occur given H_t , where H_t denotes the space-time magnitude occurrence history of the earthquakes up to time t . The same authors emphasized that H_t includes not only the earthquakes that occurred during the study time interval and in the study space window but also those that occurred before the study time interval and outside the study space window. The study time interval and the study space window are specified in Subsection 2.3.2.

In Eq. (2.1), s_{β} is the probability density function (pdf) associated with the distribution of earthquake magnitudes. It is assumed that the distribution of the magnitude of earthquakes is independent of the distributions of the occurrence time of earthquakes and the 2-D spatial location of their epicenters. It can be expressed, for arbitrary $\beta \in (0, \infty)$ as

$$s_{\beta}(m) = \beta \exp\{-\beta(m - m_0)\}, \quad (2.2)$$

where m and m_0 represent the magnitude of the earthquake and the magnitude threshold, respectively.

In Eq. (2.1), $\lambda_{\theta}(t, x, y | H_t)$ represents the rate of observation of earthquakes in time and space, given the information on earthquakes prior to time t . This rate is expressed as the sum of two terms and is defined as

$$\lambda_{\theta}(t, x, y | H_t) = \mu(x, y) + \sum_{i:t_i < t} k(m_i)g(t - t_i)f(x - x_i, y - y_i | m_i), \quad (2.3)$$

with

$$\mu(x, y) = \nu u(x, y), \quad (2.4)$$

where $\nu \in (0, \infty)$. The term $\mu(x, y)$ is usually called “background seismicity rate” and represents the rate at which earthquakes independently occur around longitude x and latitude y . The i th term of the summation in Eq. (2.3), namely

$$k(m_i)g(t - t_i)f(x - x_i, y - y_i | m_i) \quad (2.5)$$

represents the effect of the i th earthquake before time t on the occurrence rate of earthquakes that would occur at time t , with an epicenter around (x, y) . Thus,

$$\sum_{i:t_i < t} k(m_i)g(t - t_i)f(x - x_i, y - y_i | m_i)$$

describes the total effect of all the earthquakes that occurred prior to time t , on the rate at which earthquakes would occur with an epicenter around (x, y) at time t .

The expressions of k , g , and f are discussed individually as follows. First,

$$k(m) = Ae^{\alpha(m-m_0)}, \quad m \geq m_0, \quad (2.6)$$

can be interpreted as the expected number of earthquakes triggered by a previous earthquake with magnitude m , where $A \in (0, \infty)$ and $\alpha \in (0, \infty)$. Second, for all $t \in (t_i, \infty)$,

$$g(t - t_i) = \frac{p-1}{c} \left(1 + \frac{t - t_i}{c}\right)^{-p}, \quad (2.7)$$

is the pdf for the occurrence time of an earthquake triggered by the i th earthquake in the catalog, which occurred at time t_i , where $c \in (0, \infty)$ and $p \in (1, \infty)$. Third,

$$f(x - x_i, y - y_i | m_i) = \frac{q - 1}{\pi D e^{\gamma(m_i - m_0)}} \left\{ 1 + \frac{(x - x_i)^2 + (y - y_i)^2}{D e^{\gamma(m_i - m_0)}} \right\}^{-q} \quad (2.8)$$

is the pdf for the occurrence location (epicenter) of an earthquake triggered by the i th earthquake in the catalog, which occurred with magnitude m_i and an epicenter at (x_i, y_i) , where $D \in (0, \infty)$, $\gamma \in (0, \infty)$, and $q \in (1, \infty)$.

In the ETAS model, the earthquake is assumed to be either a background event, which occurs independently of previous earthquakes, or an event triggered by a previous event (Ogata, 1998). Irrespective of whether an earthquake is a background event or triggered event, it is thought to generate a non-stationary Poisson process with the intensity function defined by Eq. (2.5); see Zhuang (2011).

To simulate earthquake data from an ETAS model and make accurate forecasts, it is important to understand and capture the spatial and/or temporal clustering of earthquakes in the catalog. Therefore, a method of declustering, which requires a modeling of the clusters, is introduced in Subsection 2.3.3. Before that, the relevant terminology is defined in Subsection 2.3.2.

2.3.2 ETAS model terminology

Because of edge effects, it is highly recommended to study earthquakes based on a wider space-time window $[0, T^*) \times \mathbf{S}^*$, where $t = 0$ corresponds to a specific time origin, which is also called the 'time begin' (t_{begin}). The space-time window of interest is the study space-time window $[t_{\text{start}}, t_{\text{end}}) \times \mathbf{S} \subseteq [0, T^*) \times \mathbf{S}^*$, where the study start (t_{start}) and the study end (t_{end}) draw the limits of the study time interval, and \mathbf{S} represents the study region.

After specifying the study space-time window, the earthquakes in the catalog can be classified as target events and complementary events (Zhuang et al., 2006). The target

events are earthquakes that occurred inside the study region S and over the study interval $[t_{\text{start}}, t_{\text{start}} + T)$, where $T = t_{\text{end}} - t_{\text{start}}$. If there are other earthquakes in the catalog, which occurred before t_{start} or outside the study region S , these are classified as complementary events. Let N' denote the number of target events in the catalog. For convenience in the following subsections, the target events will be represented by the point pattern $\{(t'_i, x'_i, y'_i, m'_i), i = 1, \dots, N'\}$.

2.3.3 Stochastic declustering

Consider the earthquake catalog $\{(t_i, x_i, y_i, m_i), i = 1, \dots, N\}$. To remove the triggered events from such an earthquake catalog, [Zhuang et al. \(2002\)](#) introduced a stochastic approach to declustering earthquakes based on the 2-D spatio-temporal ETAS model, and their approach is followed in this study.

Specifically, [Zhuang et al. \(2002\)](#) proposed that for all $i < j$,

$$\rho_{i,j} = \frac{k(m_i)g(t_j - t_i)f(x_j - x_i, y_j - y_i | m_i)}{\lambda_\theta(t_j, x_j, y_j | H_{t_j})}$$

represents the probability that the j th earthquake is triggered by the i th event ($t_i < t_j$), and

$$\rho_j = \rho_{1,j} + \dots + \rho_{j-1,j} \quad (2.9)$$

represents the probability that the j th earthquake is a triggered event, which is usually called the "triggered probability".

Then, the "background probability" of the j th earthquake can be easily defined as

$$\varphi_j = 1 - \rho_j = \frac{\mu(x_j, y_j)}{\lambda_\theta(t_j, x_j, y_j | H_{t_j})}. \quad (2.10)$$

From Eq. (2.3), it is immediate that the range of values for both the triggered probability and the background probability is $[0, 1]$ for each event. If each event in the catalog

is removed randomly with the corresponding triggered probability, then the remaining events are called the "background events" and can be considered as a point pattern generated from a point process with intensity function $\mu(x, y)$ (Zhuang et al., 2002). Triggered probabilities are unknown and need to be estimated. Thus, before applying the stochastic declustering, the conditional intensity function must be estimated, and the fitting procedure for the ETAS model is described below.

2.3.4 Parameter estimation and model fitting

The 2-D spatio-temporal ETAS model is a semi-parametric model with parameters β , θ , and a nonparametric component $u(x, y)$. Consider again the earthquake catalog $\{(t_i, x_i, y_i, m_i), i = 1, \dots, N\}$, where N is the number of earthquakes in the catalog. The log-likelihood function for the 2-D spatio-temporal ETAS model is

$$\ln L(\beta, \theta) = \sum_{i=1}^N \mathbf{1}_i \ln \{ \lambda_{\beta, \theta}(t_i, x_i, y_i, m_i | H_{t_i}) \} - \int_{m_0}^{\infty} \int_{t_{\text{start}}}^{t_{\text{start}}+T} \iint_{\mathbf{S}} \lambda_{\beta, \theta}(t, x, y, m | H_t) dx dy dt dm,$$

where $\mathbf{1}_i = 1$ if the i th event is in the study space-time window and 0 otherwise (Ogata, 1998).

It can be deduced from Eq. (2.1) and the underlying assumptions, that the maximum likelihood estimate (MLE) of β has the closed-form expression

$$\hat{\beta} = \frac{N'}{\sum_{i=1}^N \mathbf{1}_i (m_i - m_0)}, \quad (2.11)$$

where $N' = \mathbb{1}_1 + \dots + \mathbb{1}_N$ is the number of target events.

The MLE of other parameters in θ cannot be calculated analytically. Zhuang et al. (2002) proposed an iterative algorithm to estimate the background seismicity rate μ and the model parameters simultaneously. Zhuang (2011) adapted it to his needs for the ETAS model studied.

2.3.4.1 Estimating the nonparametric component

Zhuang et al. (2002) proposed to estimate $\mu(x, y)$ using a variable weighted kernel based on the total spatial intensity function.

Under the conditions of stationarity and ergodicity, the total spatial intensity function is defined as

$$\Lambda(x, y) = \lim_{T_0 \rightarrow \infty} \frac{1}{T_0} \int_0^{T_0} \lambda_\theta(t, x, y | H_t) dt,$$

where T_0 is the length of the observation period. In practice, a finite approximation is used to replace the limit and substitute Eq. (2.3) in the above equation (Zhuang et al., 2002), so that

$$\begin{aligned} \Lambda(x, y) &\approx \frac{1}{T_0} \int_0^{T_0} \lambda_\theta(t, x, y | H_t) dt \\ &= \mu(x, y) + \frac{1}{T_0} \sum_{i:t_i < T_0} k(m_i) f(x - x_i, y - y_i | m_i). \end{aligned}$$

It follows that the background seismicity rate $\mu(x, y)$ can be approximated by

$$\mu(x, y) \approx \Lambda(x, y) - \frac{1}{T_0} \sum_{i:t_i < T_0} k(m_i) f(x - x_i, y - y_i | m_i). \quad (2.12)$$

For convenience, we set

$$\gamma(x, y) = \frac{1}{T_0} \sum_{i:t_i < T_0} k(m_i) f(x - x_i, y - y_i | m_i).$$

In view of Eq. (2.12), the difference between an estimate of $\Lambda(x, y)$ and an estimate of $\gamma(x, y)$ is a natural estimate of $\mu(x, y)$.

Given the observations in the time interval $[0, T_0]$, [Zhuang et al. \(2002\)](#) suggested using the variable kernel method to estimate Λ , viz.

$$\hat{\Lambda}(x, y) = \frac{1}{T_0} \sum_{i:t_i \in [0, T_0]} Z_{d_i}(x - x_i, y - y_i),$$

where $Z_{d_i}(x - x_i, y - y_i)$ is the bivariate Gaussian Kernel function, which can be written as

$$Z_{d_i}(x - x_i, y - y_i) = \frac{1}{2\pi d_i^2} \exp \left\{ -\frac{(x - x_i)^2 + (y - y_i)^2}{2d_i^2} \right\}. \quad (2.13)$$

Above, d_i represents the varying bandwidth, which is calculated for each event i as follows: for a given integer n_p and a threshold value ϵ , $d_i = \max(h_i, \epsilon)$, where h_i is the spatial distance between the i th earthquake and its n_p th closed neighbor in space. The presence of threshold ϵ is to avoid that some earthquakes overlap. [Zhuang \(2011\)](#) suggested 0.05 (degree) as a threshold, because 0.05 (degree) is close to the earthquake location error.

Using the same kernel function, $\gamma(x, y)$ can be estimated by

$$\hat{\gamma}(x, y) = \frac{1}{T_0} \sum_{i:t_i < T_0} \rho_i z_{d_i}(x - x_i, y - y_i),$$

where ρ_i is the triggered probability defined in Eq. (2.9).

Following Eq. (2.12),

$$\hat{\mu}(x, y) = \frac{1}{T_0} \sum_{i:t_i \in [0, T_0]} \varphi_i Z_{d_i}(x - x_i, y - y_i) \quad (2.14)$$

where φ_i is the background probability defined in Eq. (2.10).

The estimates of γ and μ above are called the “variable weighted kernel estimates” ([Zhuang et al., 2002](#)).

2.3.4.2 Iteration algorithm

The iterative algorithm proposed by [Zhuang \(2011\)](#) to jointly estimate the model parameters and the background seismicity rate in the ETAS model is written as Algorithm 1 below.

Algorithm 1

- 1: Initialization with given n_p and ϵ , where ϵ is a small positive number.
- 2: Calculate the bandwidth h_i of the earthquake characterized by the data vector (t_i, x_i, y_i, m_i) in the catalog, for each $i \in \{1, \dots, N\}$.
- 3: Set $\ell \leftarrow 0$ and $u^{(0)}(x, y) \leftarrow 1$.
- 4: Using the maximum likelihood procedure ([Ogata, 1998](#)), fit the ETAS model with conditional intensity function

$$\lambda_\theta(t, x, y | H_t) = \nu u^{(\ell)}(x, y) + \sum_{i:t_i < t} k(m_i) g(t - t_i) f(x - x_i, y - y_i | m_i)$$

to the earthquake data catalog, where k , g , and f are defined in Eqs. (2.6)–(2.8). The model parameters are $\theta = (\nu, A, \alpha, c, p, q, D, \gamma)$, where parameter ν is aimed to accelerate the convergence of the algorithm.

- 5: Use Eq. (2.10) to calculate φ_i for each $i \in \{1, \dots, N\}$.
 - 6: Calculate $\hat{\mu}(x, y)$ from Eq. (2.14) and record as $u^{(\ell+1)}(x, y)$.
 - 7: If $\max |u^{(\ell+1)}(x, y) - u^{(\ell)}(x, y)| > \epsilon$, then set $\ell \leftarrow \ell + 1$ and go to Step 4. Otherwise, save $\nu u^{(\ell+1)}(x, y)$ as the estimate of μ and stop.
-

Small values of n_p and ϵ can help Algorithm 1 to converge ([Zhuang, 2011](#)), and in this study, the values of n_p and ϵ are set to be 5 and 1×10^{-6} , respectively.

2.4 Earthquake data catalog

After carefully comparing existing catalogs of Canadian earthquake data, the National Earthquake Database (NEDB) was found to be the most complete, especially for earthquakes with small magnitudes (unit: moment magnitude). The NEDB collates information from the Canadian National Seismograph Network (CNSN), the Yellowknife Seismological Array (YKA), previous regional telemetered networks in eastern and western Canada (ECTN, WCTN), local telemetered networks (CLTN, SLTN), the Regional Ana-

logue Network, and the former Standard Seismograph Network (CSN). The earthquake data used for analysis in this study were downloaded from NEDB via the Earthquakes Search (On-line Bulletin) at <http://earthquakescanada.nrcan.gc.ca/stndon/NEDB-BNDS/bulletin-en.php>.

In this study, the region of interest is a space frame with longitude ranging from 126.75°W to 130.5°W and latitude ranging from 48.25°N to 49.75°N. This region is one of the most earthquake-prone areas in Canada, near Vancouver Island (British Columbia). Figure 2.1 is a geographic map of the region from Google Earth. One can see that most of this region lies in the sea.

The earthquake data catalog comes from NEDB with the space-time window covering longitude from 126.25°W to 131°W and latitude from 48°N to 50°N spatially and the period from 2000-01-01 00:00:00 to 2019-12-31 23:59:59 (UTC) temporally. Note that the depth of earthquakes of interest is from -5 km to 1000 km. In this study, the magnitude threshold is set to 3.5, and the study space-time window is constructed by the space frame: latitude from 48.25°N to 49.75°N and longitude from 126.75°W to 130.5°W, and the time period from 2008/04/27 00:00:00 to 2018/04/27 00:00:00, in which the assumptions of the ETAS model are satisfied.

The application of the ETAS model in this study presupposes that the earthquake data catalog is complete (Zhuang, 2011). It is also assumed that the stochastic process underlying the events is stationary, or at the least there is no evidence to the contrary. As stated, e.g., by Jalilian (2019), the incompleteness of the catalog and the departure from stationarity in time could cause issues in the statistical analysis, leading to unreliable results based on the fitted model. The assessment of these assumptions is reported on in the following subsections.

2.4.1 Completeness of the earthquake data catalog

Jalilian (2019) stated that when the earthquake data catalog is complete, the plot of $\log_{10}(N_{\text{mag}})$ versus magnitude mag should exhibit a linear relationship, where N_{mag} is the

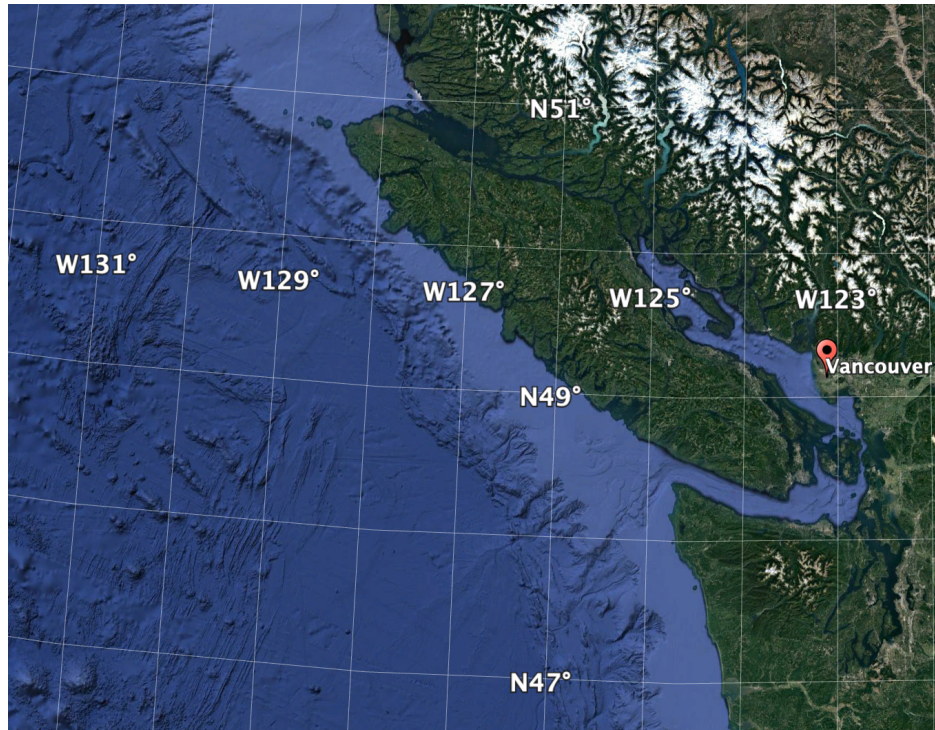


Figure 2.1: A geographic map of the region of interest in this study.

total number of earthquakes with magnitude mag or larger, and the minimum magnitude that makes this linear relationship hold can be used as magnitude threshold in the model fitting.

The plots in Figure 2.2 (a)–(d) are constructed from the subsets of earthquakes with a magnitude larger than or equal to 0, 2.5, 3.5, and 4, respectively. The expected linear pattern can be observed if $\text{mag} \geq 2.5$. This suggests that the subset of earthquakes is likely to be complete when the magnitude threshold is set to 2.5 or any larger value. Typically, the smaller the magnitude of an earthquake, the smaller the damage caused by it. Accordingly, more attention is paid to large earthquakes. Furthermore, Algorithm 1 is time consuming and takes longer to converge when a lower magnitude threshold is used. Thus, the magnitude threshold is set to be 3.5 in this study.

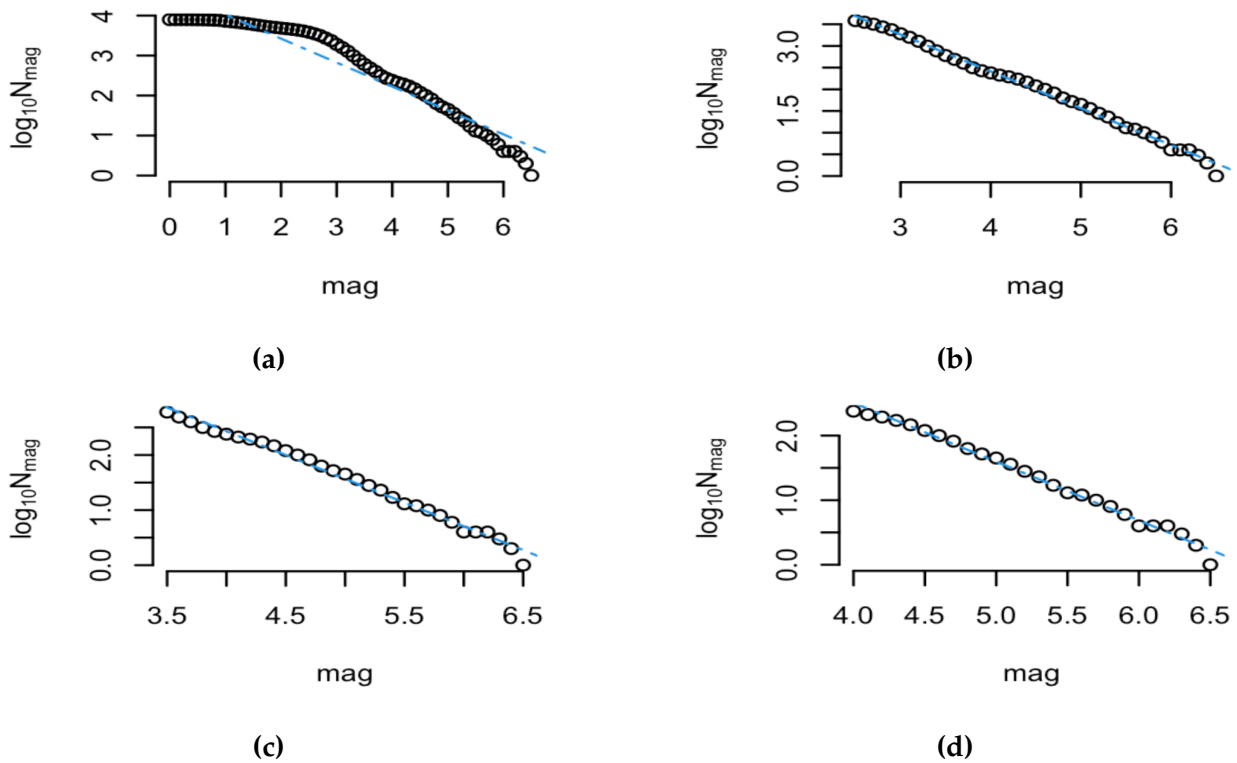


Figure 2.2: Plots of $\log_{10}(N_{\text{mag}})$ versus mag (magnitude) by increments of 0.1 from 0, 2.5, 3.5, and 4 in panels (a), (b), (c), and (d), respectively.

2.4.2 Stationarity in time

If the stochastic process underlying the events is stationary, the number of earthquakes that occurred in a given time span should only be proportional to the length of this time span. [Jalilian \(2019\)](#) proposed to plot the number of earthquakes in the catalog before time t versus time t in order to assess the stationarity in time. By convention, $t = 0$ corresponds to the start time in the catalog, i.e., 2000-01-01 00:00:00 here. When the assumption of stationarity in time holds, a linear relationship should be observed, and the beginning of the linear pattern can be used as the start of the study time interval. Note that the plot is based on the subset of earthquakes with a magnitude of 3.5 or larger, after the magnitude threshold has been determined and set to 3.5.

The resulting plot is shown in Figure 2.3, from which an approximate linear relationship between N_t and t (time) is observed over the time span defined by the two red dashed

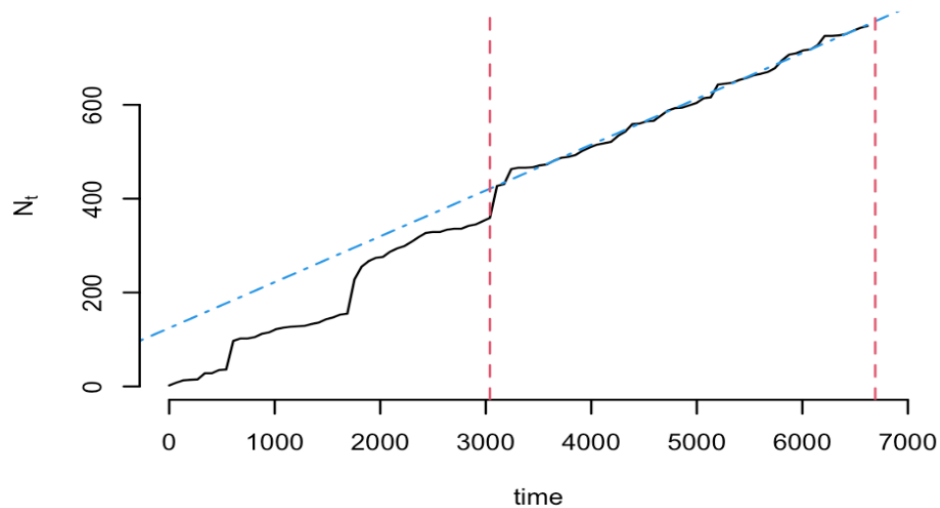


Figure 2.3: Plot of the number of earthquakes in the catalog before time t versus time t . The x -axis represents the lag (day) from the start time of the earthquake catalog, 2000/01/01 00:00:00. The left red dashed vertical line marks the 2008/04/27 00:00:00, and the right red dashed vertical line marks the end of the study period 2018/04/27 00:00:00.

vertical lines. Thus, the assumption of stationarity in time seems to be satisfied over the proposed study time interval. There is a jump in the number N_t of earthquakes just before the left red dashed vertical line, due to an earthquake with magnitude 5.1 that occurred on 2008/4/27 at 21:17:59.

2.4.3 Summary

The original earthquake data catalog was downloaded from the NEDB website. It covers the time interval from 2000-01-01 00:00:00 to 2019-12-31 23:59:59 (UTC) and the space frame from 48°N to 50°N in latitude and from 126.25°W to 131°W in longitude, with hypocenter depth from -5 km to 1000 km. The study space-time window combines the time period from 2008/04/27 00:00:00 to 2018/04/27 00:00:00 with the space frame: latitude from 48.25°N to 49.75°N; longitude from 126.75°W to 130.5°W. The magnitude threshold is set to 3.5. The resulting earthquake data catalog appears to be reasonably complete, and the stochastic process underlying the events seems stationary in the study time interval. The number of events in the study space-time window with a magnitude of

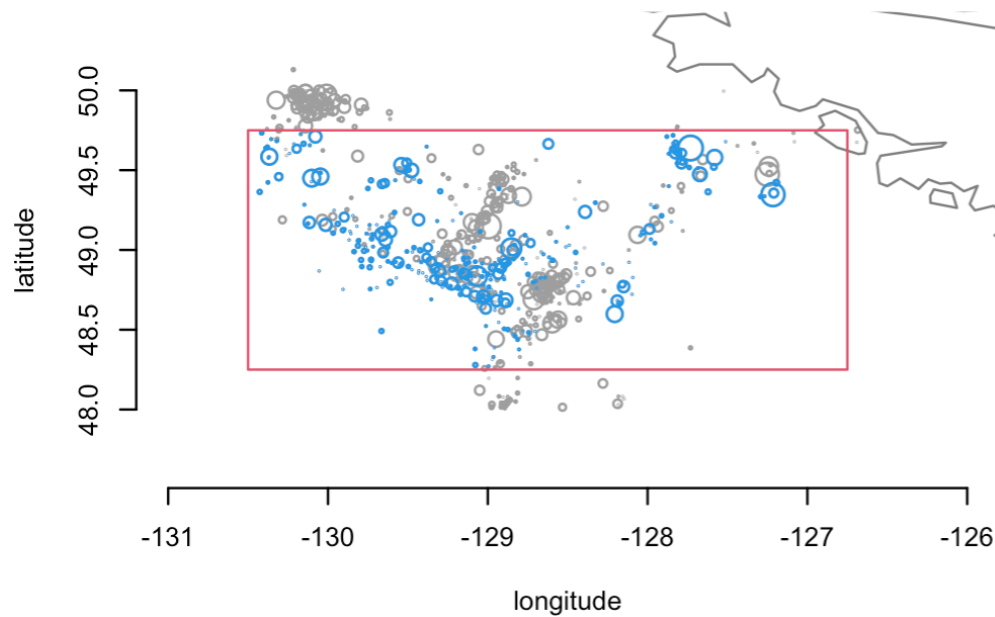


Figure 2.4: Map of the earthquakes used in the ETAS model fitting. The red frame delineates the study space window. The blue circles represent the target events while the grey circles represent the complementary events. The size of each circle is proportional to the magnitude of the corresponding earthquake.

3.5 and above is 768, including 335 target events and 433 complementary events. The geographical location of the epicenters of earthquakes with a magnitude equal to or greater than 3.5 in the catalog is shown in Figure 2.4.

2.5 The ETAS model fitting procedure

In this section, the ETAS model is fitted to the earthquake data catalog described in Section 2.4. Besides the magnitude threshold and the study space-time window, an initial value for $\theta = (\nu, A, \alpha, c, p, q, D, \gamma)$ needs to be selected carefully to start the iterative Algorithm 1. [Ogata \(1998\)](#) and [Jalilian \(2019\)](#) suggested that initially, $\nu = N/(4T|S|)$, $A = 0.01$, $c = 0.01$, $\alpha = 1$, $p = 1.3$, $D = 0.01$, $q = 2$ and $\gamma = 1$, where N is the number of events in the catalog, T is the length of the study time interval, and $|S|$ represents the projected

area (deg^2) of the study space window. The initial value of ν is calculated as 0.0142464 in this study.

It is worth emphasizing that the initial value of θ suggested by [Ogata \(1998\)](#) and [Jalilian \(2019\)](#) is a rough estimation and does not ensure that Algorithm 1 will converge. Alternatively, the ETAS model can be fitted with a higher magnitude threshold first and then, the parameter estimates thus obtained can be used as the initial values to fit the ETAS model with a lower magnitude threshold.

The ETAS model parameter estimates and their corresponding asymptotic standard errors derived from the Hessian matrix are reported in Table 2.1. Clearly, the asymptotic standard errors for parameters c , D , and γ are much larger than their respective estimates. In particular, the asymptotic standard error for parameter D is about 45 times larger than the estimate. If this large-sample approximation and the resulting estimate are deemed reliable, the parameters c , D , and γ in this ETAS model should be considered as 0 at the $\alpha = 5\%$ significance level.

[Rathbun \(1996\)](#) proved that the maximum likelihood estimators of parameters for spatio-temporal self-exciting point processes are consistent and asymptotically follow a normal distribution if the length of the time span T tends to infinity. However, for a local data set, the value of T is usually small. [Wang et al. \(2010\)](#) observed that when the space-time window of the earthquake data catalog is small, there may be a bias in the asymptotic standard errors of the ETAS model parameter estimates.

Here, the length of the study time interval is ten years (3652 days), which is relatively short in earthquake studies. Therefore, the finite-sample properties of the ETAS model's

Table 2.1: Estimates and corresponding asymptotic standard errors (SE) of the ETAS model parameters, obtained with the classical fitting procedure for the earthquake data catalog used as an example.

	β	ν	A	c	α	p	D	q	γ
Estimate	2.8632	0.6588	0.2424	0.0068	0.9771	1.2200	0.0033	2.4778	0.1718
SE	0.0245	0.0191	0.0408	0.1324	0.0341	0.0123	0.1510	0.0560	0.2713

parameter estimators and the accuracy of these asymptotic standard errors are studied by bootstrap simulation in the next section. We focus on the parameters in θ instead of parameter β because the ETAS model has a closed-form solution for the estimation of parameter β , as shown in Eq. (2.11).

2.6 A bootstrap procedure to build confidence intervals for the ETAS model parameters

Efron (1979) proposed the bootstrap as a computer-intensive method for approximating the sampling distribution of any statistic derived from a random sample. There exist parametric, nonparametric, and semiparametric versions of the bootstrap. The parametric bootstrap assumes that the probability distribution generating the data is known, but the probability distribution parameters are unknown. The parameters can be estimated from the data, e.g., by maximum likelihood. Then, each parameter in the probability distribution is replaced with the corresponding estimate, and the estimated distribution is used to simulate new data.

The parameter estimates obtained by fitting the ETAS model to the earthquake data catalog of interest were reported in Section 2.5. To study the finite-sample properties of the estimators of the ETAS model parameters and further assess the reliability of their asymptotic standard errors, the fitted ETAS model is used to generate 1000 simulated data sets. Then, an ETAS model is fitted to each simulated data set, and 1000 sets of parameter estimates and their corresponding asymptotic standard errors are thus recorded. An approximation of the finite-sample distribution of each parameter estimator is provided by the corresponding estimates from the 1000 simulated data sets, and the normality of the distribution can be assessed with the Shapiro–Wilk test.

The bootstrap procedure simulating earthquake data under the ETAS model is introduced in Subsection 2.6.1, and the bootstrap simulations are discussed in Subsection 2.6.2.

2.6.1 Bootstrap simulation procedure

Algorithm 2 is proposed to simulate earthquake data under the ETAS model, using estimated intensity functions in a given space-time window. It is adapted from Algorithm C of [Zhuang et al. \(2004\)](#), who took advantage of the availability of a real data set to which the ETAS model is fitted to make the simulated data sets more realistic.

In Algorithm 2, the magnitude of simulated events is generated from \hat{s}_β . However, the support of the Exponential distribution is $[0, \infty)$, and the lack of an upper bound in the magnitude of simulated events can cause the resulting simulation to be unstable ([Wang et al., 2010](#)). If one simulated event has a very large magnitude, it will tend to trigger a multitude of aftershocks, which will cause the size of the simulated earthquake data catalog to be unrealistically large. [Kagan and Schoenberg \(2001\)](#) introduced the tapered Exponential distribution to avoid such an issue. Alternatively, [Zhuang et al. \(2004\)](#) suggested that the magnitude of simulated earthquakes can be resampled from the collection of the magnitudes of the target events in the real earthquake data catalog, and their idea is applied in this study.

Algorithm 2

- 1: Fit the ETAS model to the studied earthquake data catalog $\{(t_i, x_i, y_i, m_i), i = 1, \dots, N\}$.
 - 2: Generate the background catalog with the estimated background seismicity rate $\hat{\mu}(x, y)$, recorded as generation 0, namely, E_0 .
 - 3: Set $\ell = 0$.
 - 4: For each event j represented by $(t_{\ell j}, x_{\ell j}, y_{\ell j}, m_{\ell j})$ in the catalog $E_\ell = \{(t_{\ell i}, x_{\ell i}, y_{\ell i}, m_{\ell i}), i = 1, \dots, N_\ell\}$, generate $N_j^{(\ell)}$ offspring $E_{\ell+1}^{(j)} = \{(t_k^{(j)}, x_k^{(j)}, y_k^{(j)}, m_k^{(j)}), k = 1, \dots, N_j^{(\ell)}\}$, where $N_j^{(\ell)}$ is a random number from the Poisson distribution with expected value $\hat{k}(m_{\ell j})$ with function k defined by Eq. (2.6), and $t_k^{(j)}, (x_k^{(j)}, y_k^{(j)})$, and $m_k^{(j)}$ are simulated from the estimated functions $\hat{g}(t - t_{\ell j}), \hat{f}(x - x_{\ell j}, y - y_{\ell j} | m_{\ell j})$, and $\hat{s}_\beta(m)$, respectively, where g, f , and s_β are defined by Eq. (2.7), Eq. (2.8) and Eq. (2.2), respectively.
 - 5: Set $E_{\ell+1} = \cup_{j \in E_\ell} E_{\ell+1}^{(j)}$.
 - 6: If $E_{\ell+1}$ is not empty, set $\ell = \ell + 1$ and go to Step 4, otherwise return $E_0 \cup \dots \cup E_\ell$.
-

At Step 2 of Algorithm 2, background events are simulated from the estimate $\hat{\mu}(x, y)$, which is semiparametric. [Zhuang et al. \(2004\)](#) stated that simulating background events directly from the estimate $\hat{\mu}(x, y)$ is difficult. In contrast, background events can be simulated from the real earthquake data catalog by applying the stochastic declustering method introduced in Subsection 2.3.3. As stated by [Zhuang et al. \(2004\)](#), using this declustering method to simulate background events can minimize the differences between the real earthquake data catalog and the simulated data set, even if the observed catalog is not stationary in time. To ensure that the spatial occurrence rate for the simulated background process is the same as $\hat{\mu}(x, y)$ in Eq. (2.14), a Gaussian deviation with zero mean and standard deviation d_j is added to the location (longitude and latitude of the epicenter) of each simulated background event j ([Zhuang et al., 2004](#)). The quantity d_j appears in Eq. (2.13) and is computed when the ETAS model is fitted. Moreover, the ETAS model assumes that the location of the background events is independent of the time of occurrence. To ensure that the assumption holds, the locations of the simulated background events are randomly reordered while keeping the order of the corresponding times.

Edge effects must be considered with great care whenever the simulation is made over a finite space-time window. When the study space-time window has been identified, the simulation needs to be made over a wider space-time region. Failure to take into account large earthquakes that occurred before the starting time of the study time interval or outside the study space window may cause the size of the simulated data catalog to be smaller than it should.

[Zhuang et al. \(2004\)](#) classified earthquakes outside the study space-time window as boundary events. Thereafter, the simulation was applied over the study space-time window by recording the union of boundary events and the simulated background events as generation 0, i.e., E_0 in Algorithm 2. After a new generation of earthquakes is simulated, only events inside the study space-time window are kept and used to simulate the next

generation. The aim of removing the simulated earthquakes outside the study space-time window is to avoid counting the edge effects twice (Zhuang et al., 2004).

The aforementioned method introduced by Zhuang is only suitable in the parametric version of the bootstrap but not in Monte Carlo simulation applied in Section 2.7. This is because the boundary earthquake data catalog contains triggered events, which can be treated as being simulated from the estimated intensity function, and the bootstrap uses exactly the estimated intensity function to simulate earthquake catalogs. However, in Monte Carlo simulation, earthquake events are simulated under the control of an intensity function with parameter values set by the user. In such a case, the triggered events in the boundary earthquake data catalog should no longer be treated as events generated from the intensity function of interest. For this reason, doing simulations over a wider space-time window (space frame: 48°N–50°N, 126.25°W–131°W; time span: 2000-01-01 00:00:00 to 2018/04/27 00:00:00 (UTC)) is preferred in this study.

2.6.2 Analysis based on the parametric bootstrap simulation

In this subsection, Algorithm 2 is applied 1000 times to generate 1000 simulated data sets, and the 1000 sets of parameter estimates obtained with the simulated data sets are denoted by $\{\hat{\beta}_i, \hat{\nu}_i, \hat{A}_i, \hat{c}_i, \hat{\alpha}_i, \hat{p}_i, \hat{D}_i, \hat{q}_i, \hat{\gamma}_i : i = 1, \dots, 1000\}$.

As per Eq. (2.1), the ETAS model pertains to the time and location of earthquakes and assumes that the probability density function of the magnitude of earthquakes does not change in space or time. Thus, in this study, more attention is paid to parameters in Eq. (2.3). As shown in Eq. (2.4), the product of parameters ν and $u(x, y)$ can be considered as a function $\mu(x, y)$, which is the background seismicity rate. Thus, the parameters of interest in this study are $A, c, \alpha, p, D, q, \gamma$, whose estimates, for simulated data set $i \in \{1, \dots, 1000\}$, are denoted by $\hat{A}_i, \hat{c}_i, \hat{\alpha}_i, \hat{p}_i, \hat{D}_i, \hat{q}_i, \hat{\gamma}_i$, and their corresponding asymptotic standard errors are denoted by $\hat{\sigma}_{A_i}, \hat{\sigma}_{c_i}, \hat{\sigma}_{\alpha_i}, \hat{\sigma}_{p_i}, \hat{\sigma}_{D_i}, \hat{\sigma}_{q_i}, \hat{\sigma}_{\gamma_i}$.

To study the finite-sample distribution of the estimators of ETAS model parameters, boxplots were drawn from the parameter estimates obtained with the 1000 simulated

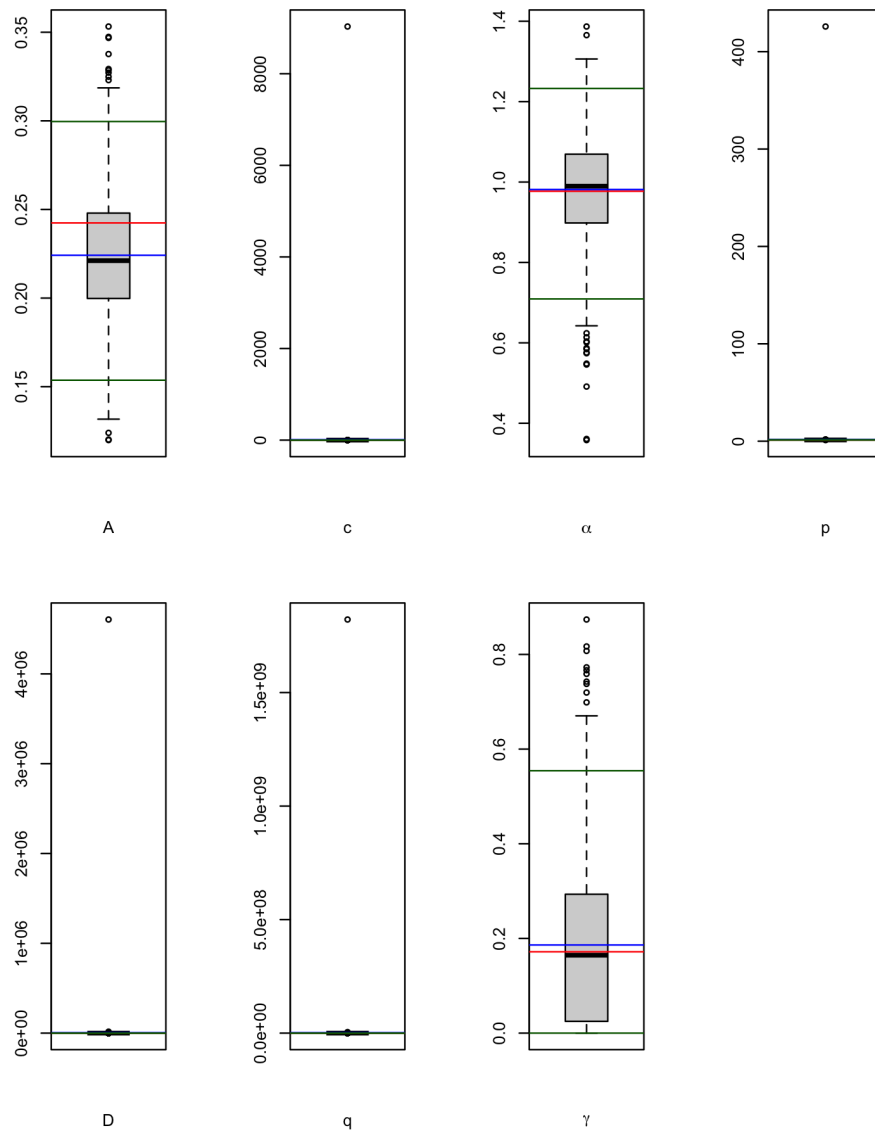


Figure 2.5: Boxplots derived from 1000 estimates (including the three extremely large outliers) obtained for seven of the ETAS model parameters by bootstrap simulation. In each boxplot, the red line represents the putative value of the corresponding parameter, the blue line marks the mean of the 1000 estimates, and the two green lines are the 2.5% and 97.5% empirical quantiles of the distribution of of the estimates, respectively.

data sets (Figure 2.5). Clearly, there are several extremely large values in the boxplots of estimates for parameters c , p , D , and q . These outliers do not affect the precision of the bootstrap confidence intervals because the latter are constructed from the 2.5% and 97.5%

Table 2.2: Three data sets with extremely large outliers obtained in bootstrap simulation.

Data set	A	c	α	p	D	q	γ
573	0.130	9031.001	0.358	425.812	7.232×10^{-14}	0.003106281	0.1603218
672	0.218	0.009	0.889	1.179	16076.52	4465327	0.288
823	0.212	0.006	1.063	1.228	4605246.56	1821736871	0.380

empirical quantiles. Nevertheless, these outliers make it difficult to assess the performance of the parameter estimation. It would be informative to identify the characteristics of the simulated data sets that lead to outliers. To this end, the parameter values of three problematic simulated data sets are reported in Table 2.2.

Among the seven parameters, more attention needs to be paid to parameters p and q in Eq. (2.7) and Eq. (2.8). It is straightforward to check that the function g is close to 0 when parameter p is very large. It means that the probability density function of the time of occurrence of triggered earthquakes nearly vanishes and the earthquakes are not clustered in time. Similarly, the function f takes tiny values when the parameter q is very large. This means that the probability density function of the geographical location of the epicenter of triggered earthquakes is approximately 0. Thus, simulated earthquakes are not clustered in space.

By comparing Figure 2.6 (simulated data set 573), Figure 2.7 (simulated data set 672), and Figure 2.8 (simulated data set 823) with Figure 2.9 (the real earthquake data catalog), one can see clearly that the earthquakes from these three simulated data sets are not clustered, whereas there are clusters of linearly aligned events in both plots at the same time for the real earthquake data catalog. This characteristic is consistent with the above discussion of the effects of large p and q , and can be used to remove extremely large outliers.

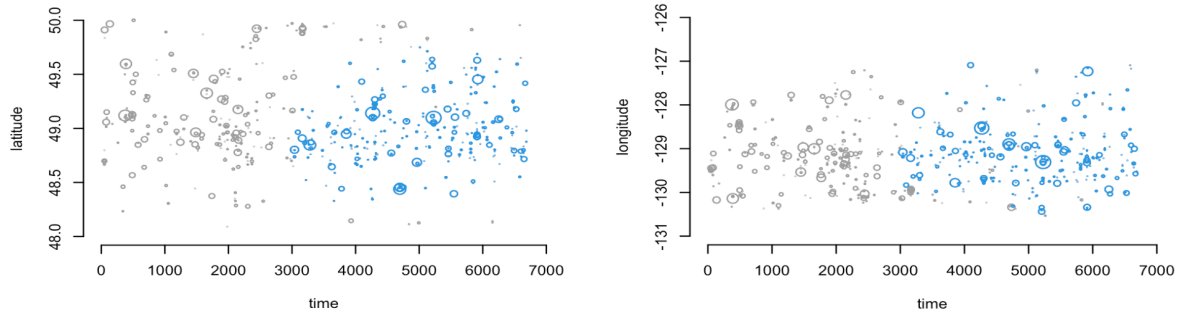


Figure 2.6: Space-time plots of the latitudes (left) and longitudes (right) against the times of occurrence of earthquakes in the simulated data set 573.

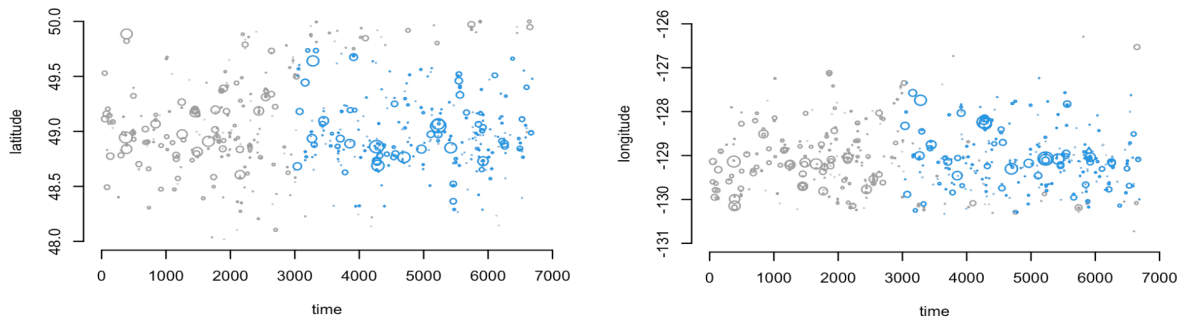


Figure 2.7: Space-time plots of the latitudes (left) and longitudes (right) against the times of occurrence of earthquakes in the simulated data set 672.

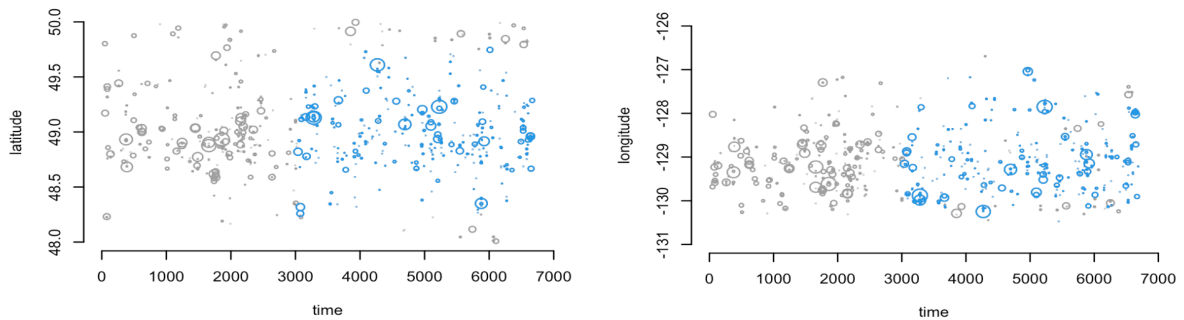


Figure 2.8: Space-time plots of the latitudes (left) and longitudes (right) against the times of occurrence of earthquakes in the simulated data set 823.

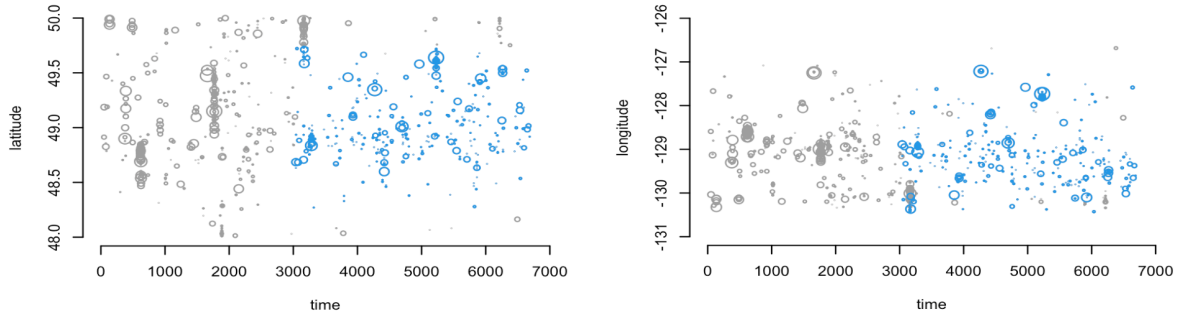


Figure 2.9: Space-time plots of the latitudes (left) and longitudes (right) against the times of occurrence of earthquakes in the real earthquake data catalog.

From Figure 2.10, it appears that the finite-sample distributions of the estimators of ETAS model parameters c , p , D , q , and γ are very skewed. Beyond these graphical observations, the Shapiro–Wilk test of normality indicates that the finite-sample distribution of these parameter estimators is not Gaussian at any reasonable level of significance; see Table 2.3. It follows that the study time interval, from 2008/04/27 to 2018/04/27 (3652 days), is not large enough for asymptotic theory to kick in, if at all.

Besides the 1000 estimates, the corresponding 1000 asymptotic standard errors were also recorded when the ETAS model was fitted to the simulated data sets. In Figure 2.11, the scale of the y -axis is as expected in the boxplots of asymptotic standard errors for parameters A , c , α , p , D , and q , whereas the scale of the y -axis of the boxplot for γ is extremely large, due to an extremely large outlier. The standard deviation of these asymptotic standard errors is also extremely large, of the order of 9.8×10^{11} (Table 2.4). To explain this, the number of asymptotic standard errors greater than 10 was counted; there are 222 such asymptotic standard errors in total. This suggests that the variation of the asymp-

Table 2.3: Observed statistic values and probabilities of significance of the Shapiro–Wilk test

	A	c	α	p	D	q	γ
W	0.99494	0.90379	0.99251	0.97337	0.54577	0.5893	0.91249
p -value	0.002021	$< 2.2 \times 10^{-16}$	6.031×10^{-5}	1.416×10^{-12}	$< 2.2 \times 10^{-16}$	$< 2.2 \times 10^{-16}$	$< 2.2 \times 10^{-16}$

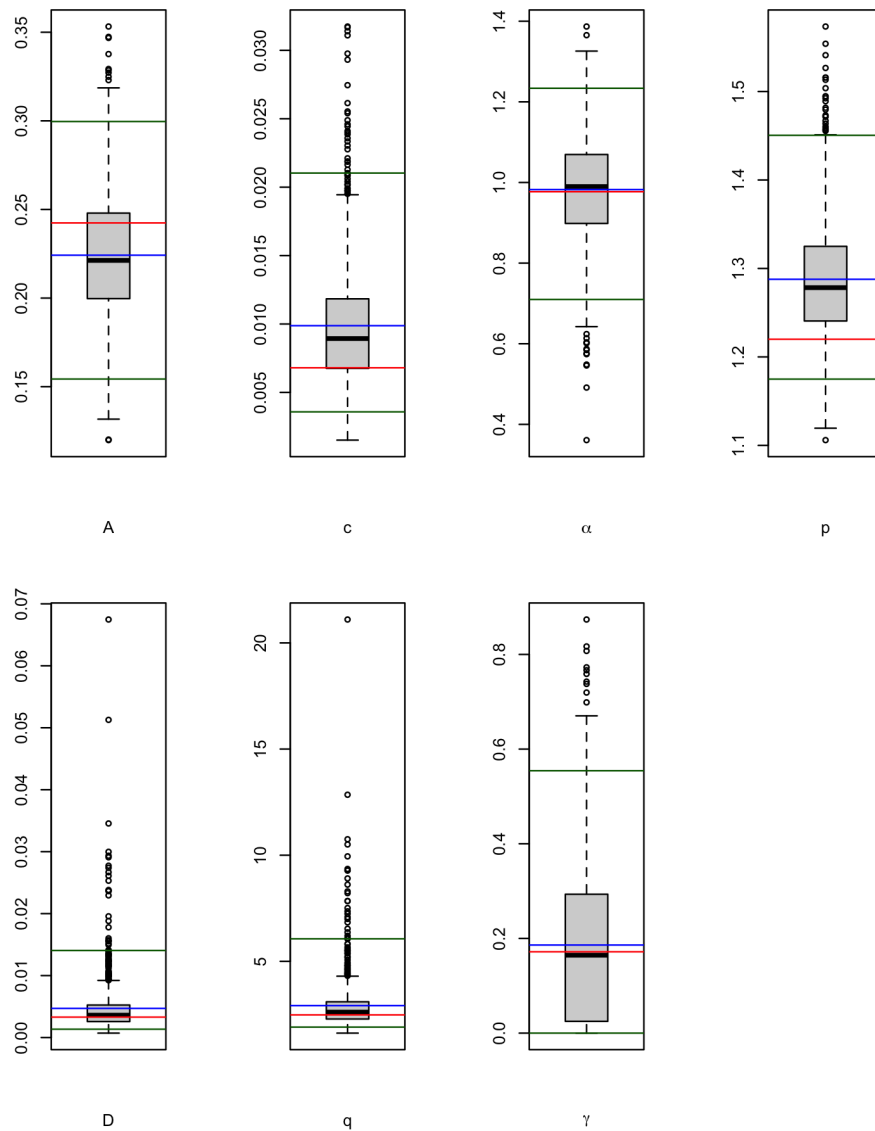


Figure 2.10: Boxplots derived from 1000 estimates (excluding the three extremely large outliers) obtained for seven of the ETAS model parameters by bootstrap simulation. In each boxplot, the red line represents the putative value of the corresponding parameter, the blue line marks the mean of the 1000 estimates, and the two green lines are the 2.5% and 97.5% empirical quantiles of the distribution of of the estimates, respectively.

otic standard error of parameter γ is large and supports that the asymptotic standard error for it is not reliable.

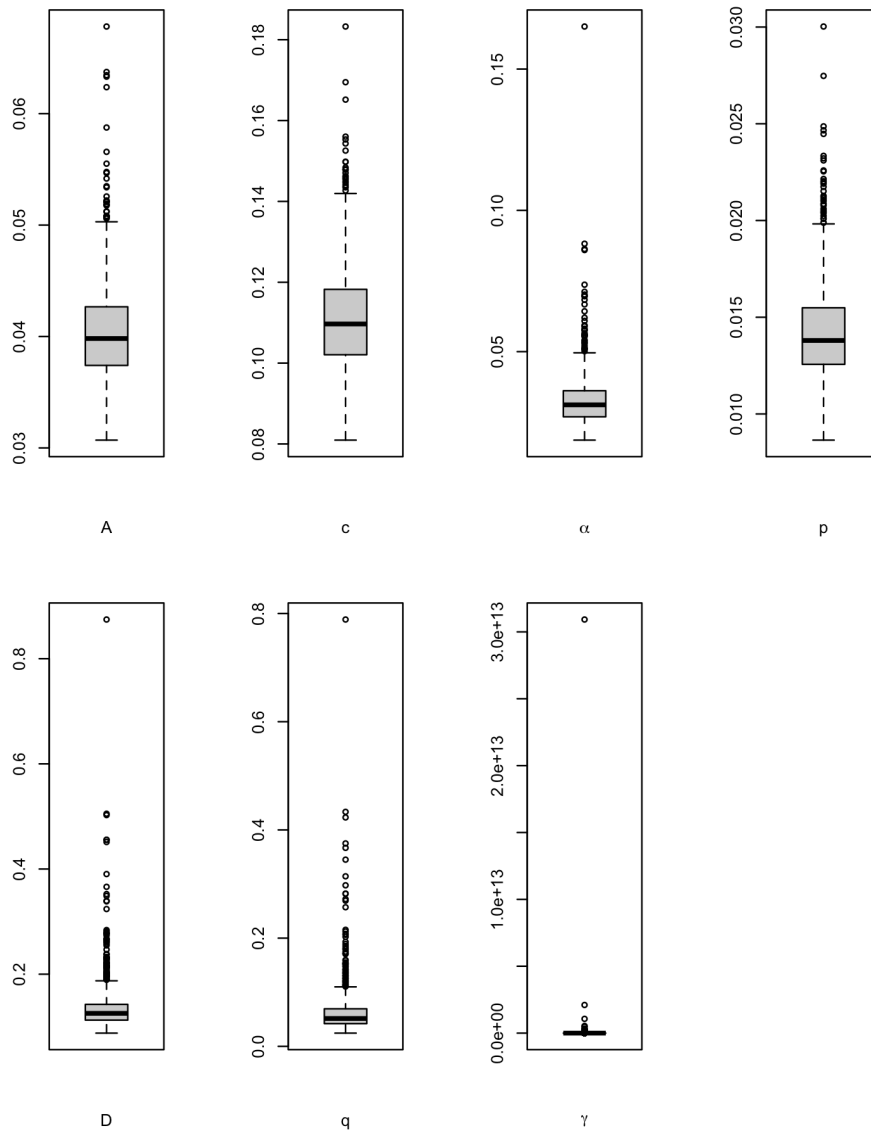


Figure 2.11: Boxplots of asymptotic standard errors of the estimates for each parameter from the 1000 simulated data sets.

Table 2.4: The standard deviation (std) of the asymptotic standard errors calculated for the 1000 simulated data sets.

	A	c	α	p	D	q	γ
Std	0.0046	0.0130	0.0094	0.0025	0.0493	0.0477	981028508310

Combining the lack of normality of the finite-sample distribution and the large variation in the asymptotic standard errors of the estimates of parameter γ , it has been shown that the asymptotic standard errors associated with the parameter estimates of a fitted ETAS model are not reliable. It follows that the asymptotic confidence interval for each parameter is also unreliable.

The standard error of a parameter estimate in the ETAS model can be approximated by the sample deviation of the 1000 parameter estimates from the simulated data sets, which is called the bootstrap standard error. Moreover, instead of the asymptotic confidence interval, the 2.5% and 97.5% empirical quantiles of the distribution of estimates from the 1000 simulated data sets lead to the 95% bootstrap confidence interval. Both bootstrap standard errors and bootstrap confidence intervals are reported in Table 2.5.

The estimate (obtained by fitting the ETAS model to the real earthquake data catalog) of each of the seven parameters is located in the corresponding 95% bootstrap confidence interval which does not contain 0. This means that the estimate of each of these parameters is different from 0 at the 5% significance level. It is also clear from Figure 2.10 that the red line is between the two green lines in each boxplot.

Table 2.5: The estimate, the asymptotic standard error (SE), the bootstrap standard error (bootstrap SE), and the 95% bootstrap confidence interval for seven parameters of the ETAS model.

	A	c	α	p	D	q	γ
Estimate	0.2424	0.0068	0.9771	1.2200	0.0033	2.4778	0.1718
SE	0.0408	0.1324	0.0341	0.0123	0.1510	0.0560	0.2713
Bootstrap SE	0.0368	0.0046	0.1324	0.0684	0.0044	1.2571	0.1678
2.5%	0.1543	0.0036	0.7098	1.1749	0.0014	1.9026	1.18×10^{-22}
97.5%	0.2996	0.0210	1.2337	1.4505	0.0141	6.0613	0.5543

2.7 A Monte Carlo simulation study

To further scrutinize the performance of the estimation procedure and confidence intervals built with the bootstrap procedure proposed in Section 2.6, a Monte Carlo simulation study is undertaken in this section.

2.7.1 Methodology

A major difference between the parametric version of the bootstrap introduced in Section 2.6 and a Monte Carlo simulation is the setting of the parameter values in the functions k , g , and f in Step 4 of Algorithm 2. For a bootstrap simulation, the parameters in k , g , and f are replaced by the corresponding estimates obtained with the real earthquake data catalog. For a Monte Carlo simulation, the target values of the parameters in k , g , and f are set by the user. Note that the same earthquake data catalog is of interest in both studies in Section 2.6 and Section 2.7, and the study space-time windows and magnitude thresholds are also the same.

For the Monte Carlo study presented in this section, the target values of parameters used to simulate earthquake data are in the same range as the parameter estimates obtained with the actual data. When the ETAS model is fitted to the real earthquake data catalog, the asymptotic standard errors of the estimates of parameters c , D , and γ are particularly large. Therefore, more attention is paid to these three parameters, and three different target values are chosen for each of them: 0.001, 0.005, and 0.01 for c ; 0.001, 0.005, and 0.01 for D ; and 0.1, 0.15, and 0.2 for γ .

The target values of the other parameters are set to be approximately equal to the corresponding estimates obtained with the real earthquake data catalog, for which $A = 0.25$, $\alpha = 1$, $p = 1.25$, and $q = 2.5$. In total, 27 combinations of simulation parameter values are considered. For each combination, Algorithm 2 is applied 1000 times to generate 1000 simulated earthquake data catalogs, and the ETAS model is fitted to each simulated

earthquake data catalog. The parameter estimates and their asymptotic standard errors are recorded.

2.7.2 Results

For the 27 combinations of target values of the model parameters, the following simulation results are reported in Tables A.1–A.27:

- a) the 2.5%, 25%, 50%, 75%, and 97.5% empirical quantiles of the distributions of parameter estimates, the mean values (Mean), and the standard deviations (Std);
- b) the observed values of statistic W of the Shapiro–Wilk test of normality and corresponding p -values;
- c) the means of asymptotic standard errors of parameter estimates (Mean of $\hat{\sigma}$), the standard deviations of asymptotic standard errors of the parameter estimates (Std of $\hat{\sigma}$), and the number of asymptotic standard errors of estimates of γ that are greater than 10 (Number of $\hat{\sigma}_\gamma > 10$).

The goal of performing the Shapiro–Wilk test is to assess the normality of the finite-sample distribution of each parameter estimator applied with Monte Carlo simulations. The corresponding p -values for parameters c , p , D , q , and γ are very small in all the 27 cases, which indicates that at any proper significance level, the finite-sample distributions of the estimators of parameters c , p , D , q , and γ in the ETAS model are not Gaussian and, as a result, that the corresponding asymptotic standard errors are not reliable. Moreover, in each case, the standard deviation of the asymptotic standard errors of the estimates of parameter γ is extremely large, and more than 100 asymptotic standard errors are greater than 10. The large variation in the asymptotic standard errors of the estimates of parameter γ indicates that the asymptotic standard error for it is not reliable. Eventually, the asymptotic confidence interval for γ also is unreliable.

Alternatively, the 95% confidence intervals deduced from the 2.5% and 97.5% quantiles or from the standard errors estimated by the standard deviations of the estimates

can be calculated and reported. Clearly, 95% confidence intervals based on the empirical 2.5% and 97.5% quantiles vary with the changing target values of parameters c , D , or γ and precisely capture the corresponding target values with no exception. Because the target values are known in each case, these results indicate that the performance of confidence intervals based on quantiles is reliable.

Furthermore, in the first nine cases, the target values of parameters are located between the empirical 25% and 75% quantiles, and are close to the 50% quantiles (medians). It implies that when the target value of parameter c is as small as 0.001, the estimation of each of the seven parameters of interest is precise. From Case 10 to Case 27, the target values of parameter p are close to, but smaller than, the corresponding 25% quantiles. This result suggests that parameter p is slightly overestimated when the target value of parameter c equals 0.005 or 0.01. Overall, the performance of the estimation procedure for the parameters of the spatio-temporal ETAS model and confidence intervals built with the proposed bootstrap procedure is reliable.

2.8 Forecasting

After verifying the performance of the estimation procedure in Section 2.7, this section aims to show how the ETAS model can be applied to make short-term forecasts of the occurrence time of aftershocks and the location of their epicenter. The forecasting is based on a simulation procedure introduced in Subsection 2.8.1, and the results of a retrospective forecasting experiment are presented in Subsection 2.8.2.

2.8.1 Simulation-based forecasting procedure

Without loss of generality, the start time of the earthquake data catalog of interest is assumed to be 0 below. For a given magnitude threshold, the data in the catalog for the n earthquakes that occurred in the space-time window $[0, t) \times \mathbf{S}$ are denoted as $\{(t_i, x_i, y_i, m_i), i = 1, \dots, N\}$. [Zhuang \(2011\)](#) proposed an algorithm to simulate earth-

Algorithm 3

-
- 1: Fit the ETAS model to the earthquake data catalog $\{(t_i, x_i, y_i, m_i), i = 1, \dots, N\}$.
 - 2: Simulate the background events in the space-time window $[t, t + \Delta t) \times \mathbf{S}$ with the estimated background intensity $\hat{\mu}(x, y)$, and record the union of these new simulated events and the events represented by $\{(t_i, x_i, y_i, m_i), i = 1, \dots, N\}$ as $E_0 = \{(t_{0i}, x_{0i}, y_{0i}, m_{0i}), i = 1, \dots, N_0\}$, where N_0 is the number of events in the union.
 - 3: Set $\ell = 0$.
 - 4: For each event j represented by $(t_{\ell j}, x_{\ell j}, y_{\ell j}, m_{\ell j})$ in the earthquake data catalog $E_\ell = \{(t_{\ell i}, x_{\ell i}, y_{\ell i}, m_{\ell i}), i = 1, \dots, N_\ell\}$, generate its $N_j^{(\ell)}$ offspring $E_{\ell+1}^{(j)} = \{(t_k^{(j)}, x_k^{(j)}, y_k^{(j)}, m_k^{(j)}), k = 1, \dots, N_j^{(\ell)}\}$, where $N_j^{(\ell)}$ is a random number from a Poisson distribution with expected value $\hat{k}(m_{\ell j})$, where k is defined in Eq. (2.6), and $t_k^{(j)}, (x_k^{(j)}, y_k^{(j)})$, and $m_k^{(j)}$ are simulated from the estimated functions $\hat{g}(t - t_{\ell j}), \hat{f}(x - x_{\ell j}, y - y_{\ell j} | m_{\ell j})$, and $\hat{s}_\beta(m)$, where g, f , and s_β are defined through Eq. (2.7), Eq. (2.8) and Eq. (2.2), respectively. Let $E_{\ell+1}'^{(j)} = \{(t_k, x_k, y_k, m_k), t_k \in [t, t + \Delta t), (x_k, y_k) \in \mathbf{S} \text{ and } (t_k, x_k, y_k, m_k) \in E_{\ell+1}^{(j)}\}$.
 - 5: Set $E_{\ell+1} = \cup_{j \in E_\ell} E_{\ell+1}'^{(j)}$.
 - 6: If $E_{\ell+1}$ is not empty, set $\ell = \ell + 1$ and go to Step 4; otherwise return $E_0 \cup \dots \cup E_\ell$.
-

quakes in the space-time window $[t, t + \Delta t) \times \mathbf{S}$, based on the information about the earthquakes in the space-time window $[0, t) \times \mathbf{S}$. Algorithm 3 here is adapted from Algorithm B of [Zhuang \(2011\)](#) and is applied in this study to simulate future earthquakes.

Step 2 of Algorithm 3 can be simplified, and the method is similar to that introduced in Subsection 2.6.1. First, the stochastic declustering method introduced in Subsection 2.3.3 is applied to identify the background events in the observed earthquake data catalog. For each background event i thus obtained, U_i is a random variable uniformly distributed in $[0, 1]$ and event i is kept if $U_i < \Delta t/t$; otherwise, event i is removed. For each remaining background event, the time of occurrence is replaced by a new time, which is uniformly distributed in the interval $[t, t + \Delta t)$, and the location is updated by adding a Gaussian deviation with zero mean and standard deviation d_i , which is the corresponding spatial bandwidth of the event. Remember that the application of the ETAS model assumes that the occurrence of earthquakes is stationary in time. That is why the value of $\Delta t/t$ above is used as a criterion to thin the obtained background events.

A bias may be introduced in the estimation of the ETAS model parameters if the edge effects are ignored. One way to reduce edge effects is to simulate earthquakes on a space frame broader than S . The simulated events in S are then separated and studied after applying Algorithm 3. This idea is implemented in this study.

To forecast earthquakes and predict their occurrence time and location (epicenter) in the space-time window $[t, t + \Delta t) \times S$, Algorithm 3 is repeatedly applied 1000 times, and 1000 simulated earthquake data catalogs are recorded. The formula for the estimated number of events in the space-time window $[t, t + \Delta t) \times S$ is given by Zhuang (2011) as

$$\begin{aligned} \hat{\mathbf{E}}\{N([t, t + \Delta t) \times S] | \text{observations before } t\} \\ = \frac{\text{total number of events in } [t, t + \Delta t) \times S \text{ in all the simulated catalogs}}{\text{number of runs of Algorithm 3}}. \end{aligned}$$

As for the estimation of the total spatial intensity function Λ (Subsection 2.3.4.1), the variable kernel method can be applied to estimate the intensity function of a point process, of which the simulated earthquake data catalogs in $[t, t + \Delta t) \times S$ are partial realizations. Specifically, the intensity function is estimated by applying the variable kernel method to the union of earthquakes in all the 1000 simulated earthquake data catalogs, each with a weight of $1/1000$. The mapping of the resulting estimated intensity function is used to predict the location (epicenter) of earthquakes in $[t, t + \Delta t) \times S$.

2.8.2 A retrospective forecasting experiment

An earthquake data catalog was downloaded from the NEDB in the ranges of longitude 126.25°W to 131°W , latitude 48°N to 50°N , time spanning from 2000/01/01 00:00:00 to 2018/11/21 00:00:00, magnitude $\text{mag} \geq 3.5$, and depth from -5 km to 1000 km. Considering the edge effects, Algorithm 3 was applied based on the space window above first, and then, the simulated earthquakes in the study space window (longitude: 126.75°W – 130.5°W , latitude: 48.25°N – 49.75°N) were separated and studied. A red rectangle depicts the study space window in Figure 2.12.

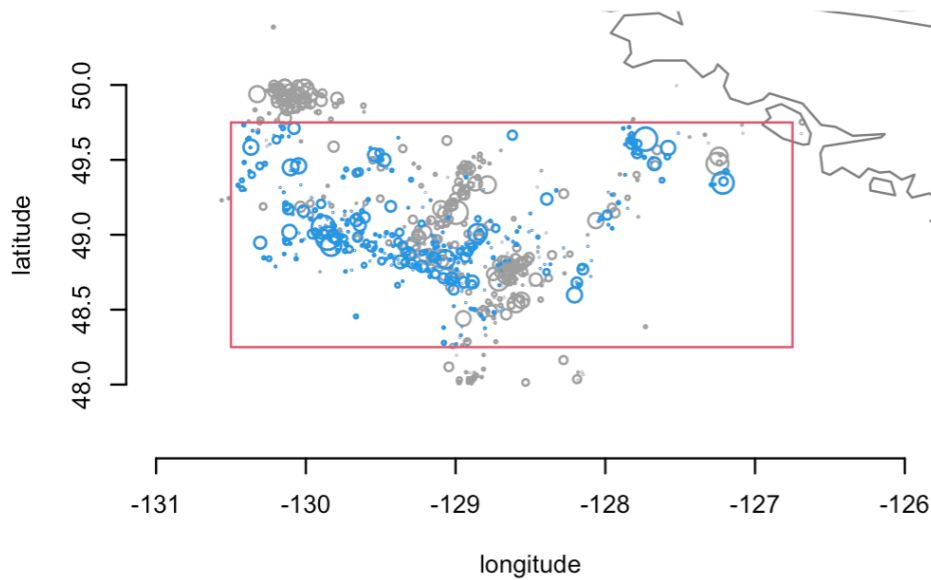


Figure 2.12: Map of earthquakes in the earthquake data catalog of interest. The blue circles represent the events in the space-time window built by space window (longitude: 126.75°W – 130.5°W , latitude: 48.25°N – 49.75°N) and time interval ([2008/04/27 00:00:00, 2018/11/21 00:00:00]), while the grey circles indicate the complementary events in the catalog. The size of each circle is proportional to the magnitude of the corresponding earthquake.

The earthquake data catalog of interest contains three large earthquakes with magnitudes above 6 on 2018/10/22. Specific spatio-temporal information about these three earthquakes is reported in Table 2.6. The retrospective forecasting experiment was performed to forecast earthquakes that occurred in the month following these large earthquakes.

Before fitting, two assumptions of the ETAS model, completeness and stationarity in time, need to be assessed on the studied earthquake data catalog. In the left graph of

Table 2.6: Three earthquakes with magnitude above 6 on the same date.

Date	Time	Longitude	Latitude	Magnitude
2018/10/22	5:39:35	-129.8310	48.9272	6.1
2018/10/22	6:16:22	-129.8540	48.9767	6.5
2018/10/22	6:22:45	-129.8831	49.0510	6.5

Fig. 2.13, the clear linear pattern after magnitude 3.5 means that the earthquake data catalog of interest can be considered complete over that range of magnitudes. In the right graph of Fig. 2.13, the relationship between N_t and time t is approximately linear over the time interval between the two red dashed vertical lines. Thus, by setting the start of the study time interval as 2008/04/27, for whatever posterior end of the study time interval, the assumption of stationarity in time is satisfied.

Zhuang (2011) stated that forecasts are better when forecasting is performed shortly after a main shock. Thus, Δt in Algorithm 3 equals 0.5 (day) and the month of interest is split into 62 half days. The first ETAS model fitted to the earthquakes that occurred prior to 2018/10/21 00:00:00 is used to forecast the earthquakes in the time span from 2018/10/21 00:00:00 to 2018/10/21 12:00:00. After completion of the first half-day forecasting, the ETAS model is fitted to the earthquakes prior to 2018/10/21 12:00:00, and the updated ETAS model is used to forecast earthquakes over the time interval spanning from 2018/10/21 12:00:00 to 2018/10/22 00:00:00. This procedure is repeated until earthquakes are forecast one month after the earthquake with magnitude 6.1 on 2018/10/22 5:39:35. The parameter estimates of each fitted ETAS model are reported in Table B.1.

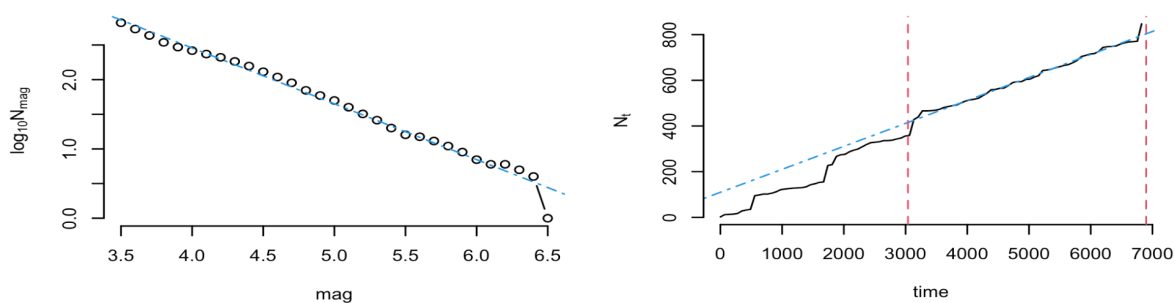


Figure 2.13: Left: Plot of $\log_{10}(N_{\text{mag}})$ versus mag (magnitude) by increments of 0.1 from 3.5. Right: Plot of N_t , the number of earthquakes (magnitude ≥ 3.5) in the catalog before time t (day), versus time t (day). The x -axis represents the lag (day) from the start time of the studied earthquake data catalog, 2000/01/01 00:00:00. The left red dashed vertical line indicates 2008/04/27 00:00:00, and the right red dashed vertical line, 2018/11/21 00:00:00, which is the last day in the earthquake data catalog.

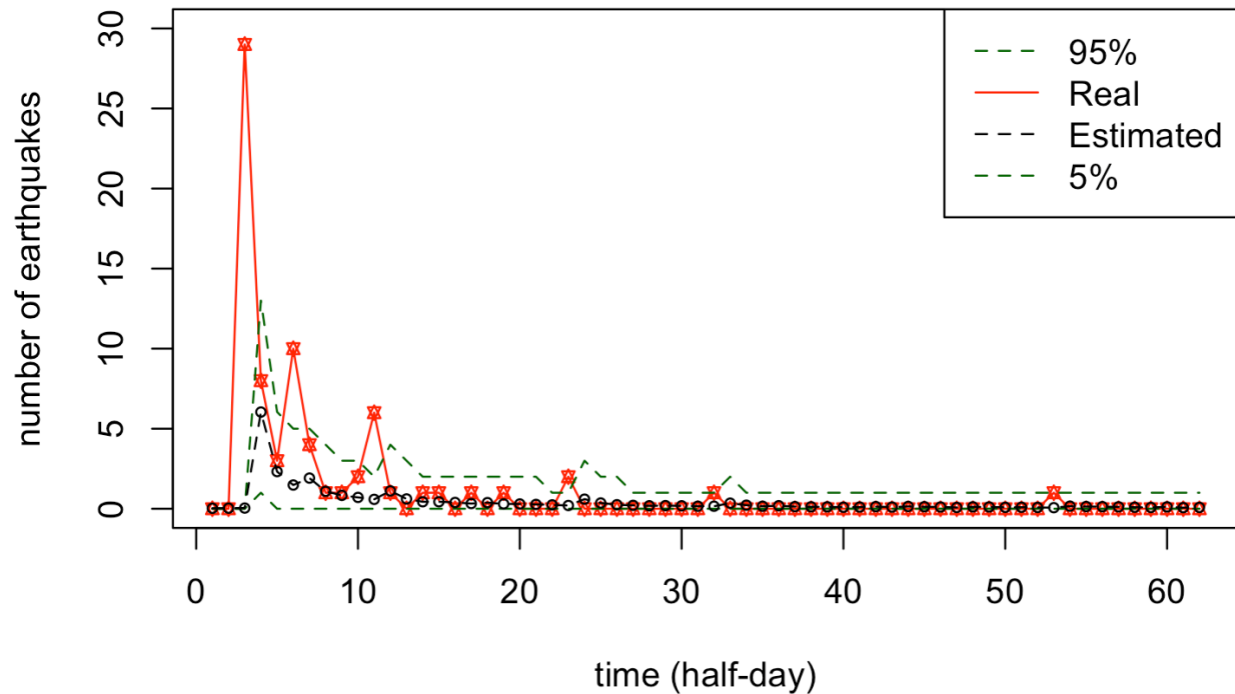
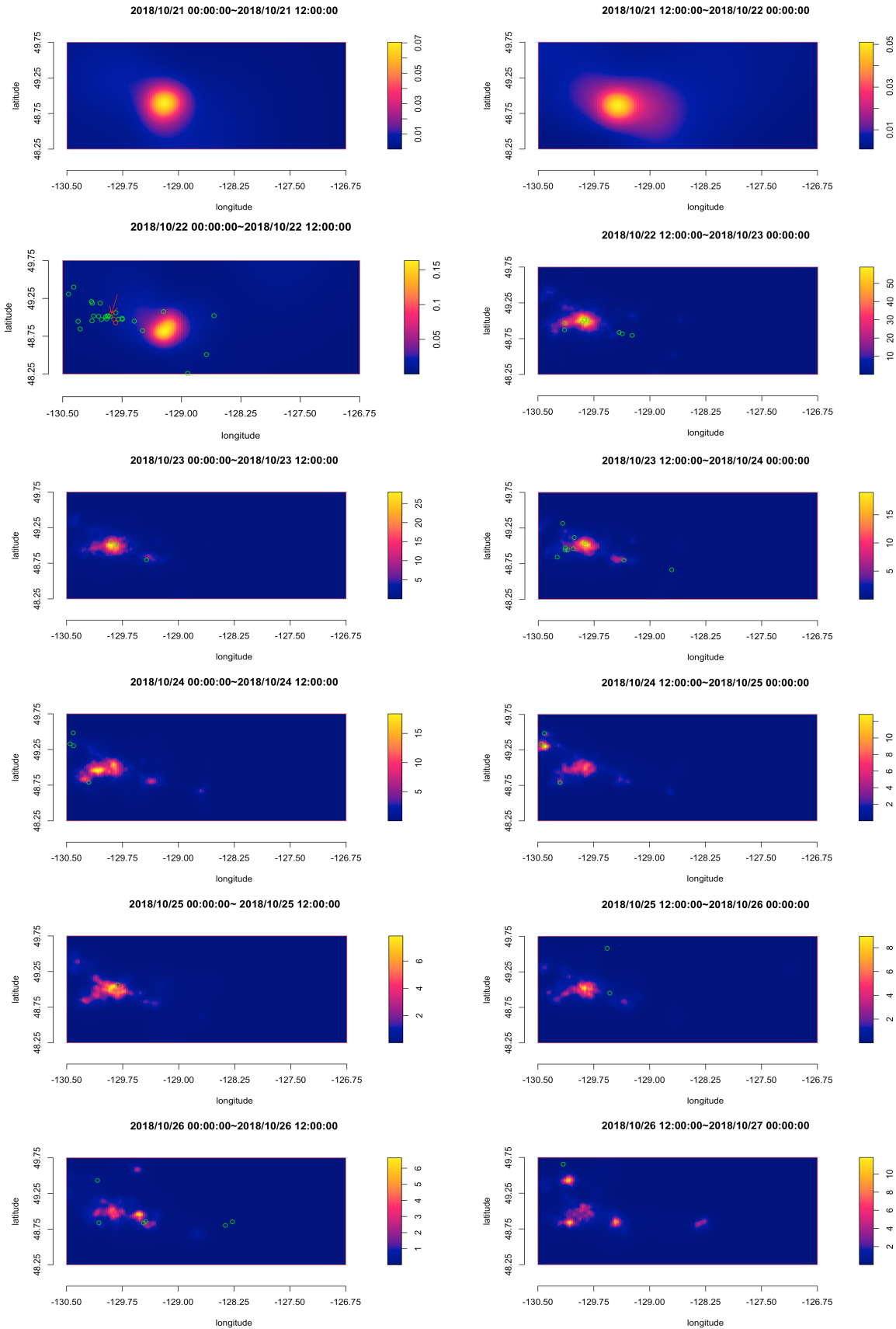


Figure 2.14: Plot against time (half-day) of the estimated half-day number of earthquakes (circles in black) in the study space window (longitude: 126.75°W – 130.5°W , latitude: 48.25°N – 49.75°N) during the time window of interest 2018/10/21 00:00:00 to 2018/11/21 00:00:00. The hexagrams indicate observed numbers of earthquakes in the corresponding half days. The lower and upper green dashed lines represent the 5% and 95% empirical quantiles of the distribution of numbers of simulated earthquakes, respectively. Integer $j \in \{1, \dots, 62\}$ on the x -axis indicates that the forecast is for the j th half day after 2018/10/21 00:00:00.

From Figure 2.14, it is clear that the forecast can accurately estimate the number of earthquakes in the one month after the three large earthquakes, excluding the time intervals [2018/10/23 12:00:00, 2018/10/24 00:00:00), [2018/10/26 00:00:00, 2018/10/26 12:00:00), and [2018/11/01 00:00:00, 2018/11/01 12:00:00). The forecast undercount may be due to some other spontaneously occurred earthquakes in these time intervals.

From Figure 2.15, it appears that the location of earthquakes after the three large earthquakes has been well forecast, especially over the time interval [2018/10/22 12:00:00, 2018/10/24 00:00:00).



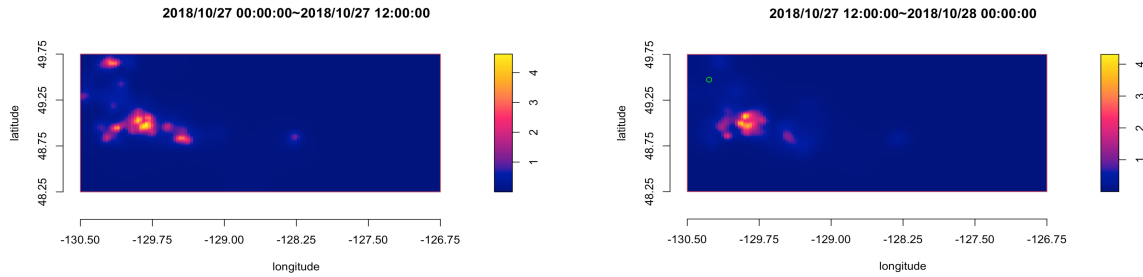


Figure 2.15: Examples of mapping the estimated intensity function (unit: events/(half-day \times deg²)) over the corresponding time intervals in the study space window to predict the location (epicenter) of earthquakes. In some panels, green circles point to the locations of earthquakes (mag ≥ 3.5) observed. The three red circles in the left graph on the second row indicate the three large earthquakes (mag ≥ 6.0).

2.9 Discussion: Use of the bootstrap procedure for Monte Carlo simulations

This section aims to further compare: (i) the asymptotic standard errors and bootstrap standard errors of the estimators of the ETAS model parameters; (ii) the confidence intervals built using the asymptotic standard errors and bootstrap confidence intervals obtained from the 2.5% and 97.5% empirical quantiles. The real earthquake data catalog (Section 2.4) continues to be used, with all the related settings, including the study space-time window and magnitude threshold.

Algorithm 2 is applied to generate 40 Monte Carlo simulations, using the ETAS model parameter estimates reported in Table 2.1 as target values. Then, the ETAS model is fitted to each of the 40 Monte Carlo simulations, and the new parameter estimates and corresponding asymptotic standard errors are recorded. For each Monte Carlo simulation, 1000 bootstrap simulations are made with Algorithm 2, using the parameter estimates of the ETAS model fitted to the current Monte Carlo simulation as putative values. An ETAS model is fitted to each bootstrap simulation, and 1000 estimates are thus recorded

for each parameter. Eventually, one bootstrap standard error per parameter is obtained for the current Monte Carlo simulation.

From the comparison of Tables C.1 and C.2, it appears that the asymptotic standard error associated with the estimate of parameter γ is extremely large for 9 of the 40 Monte Carlo simulations, while all the bootstrap standard errors computed for parameter γ are several orders of magnitude smaller; in contrast, the bootstrap standard errors for parameters D and q are excessively large for a majority of the 40 Monte Carlo simulations. Such atypical values for standard errors are due to the presence of outliers, as already discussed in Sections 2.6 and 2.7. Fortunately for the bootstrap procedure (see below), bootstrap confidence intervals can be obtained from empirical quantiles.

Under the assumption that the asymptotic distribution of the estimators of parameters in the ETAS model is Gaussian, the lengths of 95% asymptotic confidence intervals for the seven parameters studied are calculated and reported in Table C.3. As in Section 2.6, 95% bootstrap confidence intervals are built from the 2.5% and 97.5% empirical quantiles of the distributions of parameter estimates and the lengths (40 values and one mean per parameter) are reported in Table C.4.

Table 2.7 provides a summary and the basis for a final discussion. From the comparison of Tables C.3 and C.4, it is clear that the bootstrap procedure has solved the problem of unreliable asymptotic confidence intervals for γ . In view of Tables C.4 and 2.7, there is no apparent problem with the length of the 95% bootstrap confidence intervals for D ; only the 95% bootstrap confidence intervals for q are wider than the 95% asymptotic confidence intervals, overall and on average, for this parameter. For the remaining four

Table 2.7: Ratios of the mean length of 95% asymptotic confidence intervals (Table C.3) against the mean length of 95% bootstrap confidence intervals (Table C.4) for each of the seven ETAS model parameters studied.

	A	c	α	p	D	q	γ
Ratio	1.2599	20.6635	0.2396	0.1629	20.9693	0.0250	9358636018

parameters, the length ratio is smaller for bootstrap with c , shows little difference with A , and is smaller for asymptotic with α and p (Table 2.7).

In closing, though limited, this last simulation study showed variability in the results of the bootstrap procedure, but its confirmed flexibility, through the use of empirical quantiles to build confidence intervals for parameters, makes it an even more recommendable procedure in future studies involving the fitting of ETAS models to earthquake data catalogs, real or simulated.

Chapter 3

Conclusion

As mentioned in Chapter 2, self-exciting spatio-temporal point processes have been well-developed and used to study the occurrence of earthquakes, the dynamic trend of crime, the spread of infectious diseases, and so on. The object of this thesis is the 2-D spatio-temporal ETAS model, which has been widely applied to decluster earthquake data catalogs and, to a lesser degree, assess the risk of the occurrence of aftershocks.

In this thesis, an earthquake data catalog with records of earthquakes that occurred in the time span from 2000-01-01 00:00:00 to 2019-12-31 23:59:59 (UTC), in the space window: latitude from 48°N to 50°N, and longitude from 126.25°W to 131°W, and in depth from -5 km to 1000 km, was analyzed using the ETAS model. After fitting the ETAS model to the earthquake data catalog, the asymptotic standard errors for parameters c , D , and γ were found to be much larger than the corresponding estimates. From a theoretical perspective, the maximum likelihood estimators of parameters for spatio-temporal self-exciting point processes have been proved by [Rathbun \(1996\)](#) to be consistent and asymptotically normally distributed as the length of the time span tends to infinity. However, the time interval of the local earthquake data catalogs is usually short and limited.

Thus, a bootstrap procedure was proposed in this thesis to study the sampling behavior of the estimators of the parameters in the ETAS model. Using this new procedure, the hypothesis that the finite-sample distributions of the estimators of the parameters c ,

α , p , D , q , and γ are Gaussian was rejected at any reasonable significance level and, as a result, the asymptotic standard errors are not reliable. In such a case, the proposed procedure provides an alternative way to compute bootstrap confidence intervals and bootstrap standard errors for the parameters in the ETAS model.

The performance of the proposed bootstrap confidence intervals and the estimation procedures was shown to be good through a study based on Monte Carlo simulations. Then, a retrospective forecasting experiment was carried out to show how the ETAS model can be used to forecast short-term aftershocks using subsets of the real earthquake data catalog, with bootstrap results in support. In the last part of the thesis, repetitions of the bootstrap procedure with 1000 bootstrap simulations for 40 Monte Carlo simulations were used to compare the asymptotic standard errors and the bootstrap standard errors, as well as the asymptotic confidence intervals and the bootstrap confidence intervals obtained from empirical quantiles.

As introduced in Section 2.3, the conditional intensity function of the 2-D spatio-temporal ETAS model can be expressed as

$$\lambda_{\beta,\theta}(t, x, y, m | H_t) = s_{\beta}(m)\lambda_{\theta}(t, x, y | H_t),$$

where

$$\lambda_{\theta}(t, x, y | H_t) = \mu(x, y) + \sum_{i:t_i < t} k(m_i)g(t - t_i)f(x - x_i, y - y_i | m_i).$$

The formulas that are used for s_{β} , k , g , and f in this thesis were proposed by [Zhuang \(2011\)](#), and the function f is taken to be an inverse-power density. In fact, the ETAS model may take various parametric forms to represent earthquakes with different features. In contrast, [Zhuang et al. \(2002\)](#) used the light-tail Gaussian density for f , which is defined

as

$$f(x, y | m) = \frac{1}{2\pi\sigma(m)} \exp \left\{ -\frac{x^2 + y^2}{2\sigma(m)} \right\},$$

where $\sigma(m) = D \exp\{\gamma(m - m_0)\}$, in which m_0 is the magnitude threshold. Adjusting the procedures presented in this thesis to this case is straightforward.

With the development of the ETAS model, researchers have come to replace earthquake aftershocks with other events to develop self-exciting spatio-temporal point process models in other fields. For example, [Mohler \(2014\)](#) developed a self-exciting point process model to study homicides and gun crimes in Chicago. The bootstrap procedure proposed in this thesis could be applied in such contexts to study the finite-sample properties of the parameter estimators and provide alternative confidence intervals.

References

- Davis, S. D. and C. Frohlich (1991). Single-link cluster analysis, synthetic earthquake catalogues, and aftershock identification. *Geophysical Journal International* 104(2), 289–306.
- Efron, B. (1979). Bootstrap methods: Another look at the Jackknife. *The Annals of Statistics* 7(1), 1–26.
- Gardner, J. and L. Knopoff (1974). Is the sequence of earthquakes in Southern California, with aftershocks removed, Poissonian? *Bulletin of the Seismological Society of America* 64(5), 1363–1367.
- González, J. A., F. J. Rodríguez-Cortés, O. Cronie, and J. Mateu (2016). Spatio-temporal point process statistics: A review. *Spatial Statistics* 18, 505–544.
- Hawkes, A. G. (1971). Spectra of some self-exciting and mutually exciting point processes. *Biometrika* 58(1), 83–90.
- Hawkes, A. G. and L. Adamopoulos (1973). Cluster models for earthquakes-regional comparisons. *Bulletin of the International Statistical Institute* 45(3), 454–461.
- Jalilian, A. (2019). ETAS: An R package for fitting the space-time ETAS model to earthquake data. *Journal of Statistical Software* 88, 1–39.
- Kagan, Y., P. Bird, and D. Jackson (2010). Earthquake patterns in diverse tectonic zones of the globe. *Pure and Applied Geophysics* 167(6), 721–741.

- Kagan, Y. Y. and F. Schoenberg (2001). Estimation of the upper cutoff parameter for the tapered Pareto distribution. *Journal of Applied Probability* 38(A), 158–175.
- Mohler, G. (2014). Marked point process hotspot maps for homicide and gun crime prediction in Chicago. *International Journal of Forecasting* 30(3), 491–497.
- Ogata, Y. (1988). Statistical models for earthquake occurrences and residual analysis for point processes. *Journal of the American Statistical Association* 83(401), 9–27.
- Ogata, Y. (1998). Space-time point-process models for earthquake occurrences. *Annals of the Institute of Statistical Mathematics* 50(2), 379–402.
- Oluwafemi, J., O. Ofuyatan, O. Sadiq, S. Oyebisi, J. Abolarin, and K. Babaremu (2018). Review of world earthquakes. *International Journal of Civil Engineering and Technology* 9(9), 440–64.
- Rathbun, S. L. (1996). Asymptotic properties of the maximum likelihood estimator for spatio-temporal point processes. *Journal of Statistical Planning and Inference* 51(1), 55–74.
- Reasenber, P. (1985). Second-order moment of central California seismicity, 1969–1982. *Journal of Geophysical Research: Solid Earth* 90(B7), 5479–5495.
- Reinhart, A. (2018). A review of self-exciting spatio-temporal point processes and their applications. *Statistical Science* 33(3), 299–318.
- Shapiro, S. S. and M. B. Wilk (1965). An analysis of variance test for normality (complete samples). *Biometrika* 52(3/4), 591–611.
- Utsu, T. (1970). Aftershocks and earthquake statistics (1): Some parameters which characterize an aftershock sequence and their interrelations. *Journal of the Faculty of Science, Hokkaido University. Series 7, Geophysics* 3(3), 129–195.
- Wang, Q., F. P. Schoenberg, and D. D. Jackson (2010). Standard errors of parameter estimates in the ETAS model. *Bulletin of the Seismological Society of America* 100(5A), 1989–2001.

- Zhuang, J. (2011). Next-day earthquake forecasts for the Japan region generated by the ETAS model. *Earth, Planets and Space* 63(3), 207–216.
- Zhuang, J., Y. Ogata, and D. Vere-Jones (2002). Stochastic declustering of space-time earthquake occurrences. *Journal of the American Statistical Association* 97(458), 369–380.
- Zhuang, J., Y. Ogata, and D. Vere-Jones (2004). Analyzing earthquake clustering features by using stochastic reconstruction. *Journal of Geophysical Research: Solid Earth* 109(B5).
- Zhuang, J., Y. Ogata, and D. Vere-Jones (2006). Diagnostic analysis of space-time branching processes for earthquakes. In *Case Studies in Spatial Point Process Modeling*, pp. 275–292. Springer.

Appendix A

Table A.1: Case 1

	A	c	α	p	D	q	γ
Target value	0.25	0.001	1	1.25	0.001	2.5	0.1
2.5%	0.1831	5×10^{-4}	0.7748	1.192	5×10^{-4}	1.995	2.59×10^{-23}
25%	0.2205	9×10^{-4}	0.9233	1.2447	8×10^{-4}	2.3215	1.48×10^{-17}
50%	0.2446	0.0011	0.9981	1.2744	0.001	2.5534	0.0953
75%	0.2661	0.0015	1.0744	1.3098	0.0014	2.9261	0.2048
97.5%	0.3052	0.0022	1.2373	1.3846	0.0028	4.4466	0.4167
Mean	0.2439	0.0012	0.9992	1.2792	0.0012	2.7146	0.1231
Std	0.0324	4×10^{-4}	0.1166	0.0496	6×10^{-4}	0.6596	0.1252
W	0.99774	0.95518	0.99698	0.98705	0.76236	0.77095	0.87841
p -value	0.1895	$< 2.2 \times 10^{-16}$	0.05506	9.958×10^{-8}	$< 2.2 \times 10^{-16}$	$< 2.2 \times 10^{-16}$	$< 2.2 \times 10^{-16}$
Mean of $\hat{\sigma}$	0.0334	0.0935	0.0286	0.01	0.1064	0.0449	32373556581
Std of $\hat{\sigma}$	0.0029	0.0010	0.0062	0.0014	0.02110	0.0192	418803922058

Number of $\hat{\sigma}_\gamma > 10$

299

Table A.2: Case 2

	A	c	α	p	D	q	γ
Target value	0.25	0.001	1	1.25	0.001	2.5	0.15
2.5%	0.1824	6×10^{-4}	0.7531	1.1919	5×10^{-4}	1.9882	2.9485×10^{-23}
25%	0.2258	9×10^{-4}	0.9209	1.2446	8×10^{-4}	2.2909	0.0193
50%	0.2466	0.0011	1.0003	1.2755	0.001	2.5549	0.1395
75%	0.2686	0.0014	1.0664	1.3086	0.0014	2.8784	0.2555
97.5%	0.3096	0.0024	1.216	1.3881	0.0029	4.3624	0.473
Mean	0.2466	0.0012	0.9937	1.279	0.0012	2.7115	0.1610
Std	0.0322	5×10^{-4}	0.1160	0.0495	8×10^{-4}	0.7709	0.1433
W	0.99909	0.92899	0.9938	0.98269	0.62945	0.63419	0.9172
p -value	0.9158	$< 2.2 \times 10^{-16}$	0.0003686	1.621×10^{-9}	$< 2.2 \times 10^{-16}$	$< 2.2 \times 10^{-16}$	$< 2.2 \times 10^{-16}$
Mean of $\hat{\sigma}$	0.0332	0.0933	0.0288	0.0099	0.1075	0.0456	47288022580
Std of $\hat{\sigma}$	0.0028	0.0010	0.0066	0.0015	0.02650	0.0248	617296912336
Number of $\hat{\sigma}_\gamma > 10$	227						

Table A.3: Case 3

	A	c	α	p	D	q	γ
Target value	0.25	0.001	1	1.25	0.001	2.5	0.2
2.5%	0.1802	5×10^{-4}	0.7538	1.1972	5×10^{-4}	1.9967	2.1098×10^{-22}
25%	0.2226	9×10^{-4}	0.9186	1.2446	8×10^{-4}	2.3109	0.0613
50%	0.2433	0.0011	0.9951	1.2755	0.001	2.5446	0.1944
75%	0.2663	0.0015	1.0654	1.3064	0.0014	2.9266	0.3088
97.5%	0.3074	0.0024	1.2318	1.3762	0.0032	4.4546	0.5714
Mean	0.2445	0.0012	0.9935	1.2782	0.0012	2.7267	0.2021656
Std	0.0325	5×10^{-4}	0.1163	0.0482	9×10^{-4}	0.8655	0.1588
W	0.9975	0.90772	0.99583	0.98164	0.565	0.53732	0.94384
p -value	0.1289	$< 2.2 \times 10^{-16}$	0.008366	6.577×10^{-10}	$< 2.2 \times 10^{-16}$	$< 2.2 \times 10^{-16}$	$< 2.2 \times 10^{-16}$
Mean of $\hat{\sigma}$	0.0334	0.0943	0.0289	0.01	0.1088	0.0464	18295566644
Std of $\hat{\sigma}$	0.0029	0.0103	0.0064	0.0014	0.0290	0.0273	408386644591
Number of $\hat{\sigma}_\gamma > 10$	155						

Table A.4: Case 4

	A	c	α	p	D	q	γ
Target value	0.25	0.001	1	1.25	0.005	2.5	0.1
2.5%	0.1843	6×10^{-4}	0.7714	1.1989	0.0022	1.9496	1.0133×10^{-23}
25%	0.2198	9×10^{-4}	0.9226	1.2525	0.0039	2.2729	7.8021×10^{-18}
50%	0.2415	0.0012	1.0012	1.2822	0.0051	2.5277	0.0827
75%	0.2638	0.0015	1.0741	1.3216	0.0069	2.9209	0.1965
97.5%	0.3078	0.0025	1.2023	1.4179	0.0136	4.3106	0.4489
Mean	0.242	0.0013	0.9971	1.2889	0.006	2.7145	0.1184
Std	0.0319	5×10^{-4}	0.1115	0.0543	0.004	0.8602	0.132
W	0.99753	0.92191	0.99547	0.9776	0.61079	0.59105	0.84637
p -value	0.1368	$< 2.2 \times 10^{-16}$	0.00465	2.724×10^{-11}	$< 2.2 \times 10^{-16}$	$< 2.2 \times 10^{-16}$	$< 2.2 \times 10^{-16}$
Mean of $\hat{\sigma}$	0.0345	0.0963	0.0291	0.0112	0.1126	0.0487	105306470173
Std of $\hat{\sigma}$	0.0030	0.0108	0.0064	0.0018	0.0373	0.0354	1.6705×10^{12}
Number of $\hat{\sigma}_\gamma > 10$	155						

Table A.5: Case 5

	A	c	α	p	D	q	γ
Target value	0.25	0.001	1	1.25	0.005	2.5	0.15
2.5%	0.1787	5×10^{-4}	0.7442	1.1968	0.0022	1.944	1.5862×10^{-22}
25%	0.2188	9×10^{-4}	0.9287	1.252	0.004	2.307	0.0183
50%	0.2404	0.0012	1.0065	1.284	0.0053	2.5753	0.1391
75%	0.2623	0.0015	1.0735	1.3186	0.0073	2.9537	0.259
97.5%	0.3087	0.0025	1.2135	1.4012	0.0148	4.5193	0.4662
Mean	0.2414	0.0013	0.9981	1.288	0.0062	2.7447	0.1589
Std	0.0331	5×10^{-4}	0.1169	0.0528	0.0042	0.8433	0.1439
W	0.99501	0.9328	0.99092	0.98484	0.60393	0.61207	0.91191
p -value	0.002265	$< 2.2 \times 10^{-16}$	7.706×10^{-6}	1.124×10^{-8}	$< 2.2 \times 10^{-16}$	$< 2.2 \times 10^{-16}$	$< 2.2 \times 10^{-16}$
Mean of $\hat{\sigma}$	0.0347	0.0965	0.0293	0.0112	0.1135	0.0492	177927615958
Std of $\hat{\sigma}$	0.0030	0.0104	0.0071	0.0017	0.0251	0.0240	5.1689×10^{12}
Number of $\hat{\sigma}_\gamma > 10$	223						

Table A.6: Case 6

	A	c	α	p	D	q	γ
Target value	0.25	0.001	1	1.25	0.005	2.5	0.2
2.5%	0.1785	5×10^{-4}	0.7525	1.1862	0.0024	1.9648	1.309×10^{-21}
25%	0.2199	9×10^{-4}	0.9155	1.2441	0.004	2.322	0.0696
50%	0.2433	0.0011	0.9869	1.2808	0.0053	2.5723	0.1925
75%	0.2673	0.0015	1.0669	1.3198	0.0074	2.9615	0.3165
97.5%	0.3151	0.0023	1.2014	1.4131	0.0154	4.4641	0.5364
Mean	0.2441	0.0012	0.9876	1.2857	0.0063	2.7539	0.2061
Std	0.0347	5×10^{-4}	0.1136	0.059	0.004	0.8206	0.1584
W	0.99848	0.93536	0.9978	0.98129	0.70082	0.64553	0.94894
p -value	0.5428	$< 2.2 \times 10^{-16}$	0.2098	4.934×10^{-10}	$< 2.2 \times 10^{-16}$	$< 2.2 \times 10^{-16}$	$< 2.2 \times 10^{-16}$
Mean of $\hat{\sigma}$	0.0347	0.0973	0.0295	0.0112	0.1144	0.0495	15259318200
Std of $\hat{\sigma}$	0.0031	0.0110	0.0063	0.0019	0.0255	0.0247	328275056037
Number of $\hat{\sigma}_\gamma > 10$	140						

Table A.7: Case 7

	A	c	α	p	D	q	γ
Target value	0.25	0.001	1	1.25	0.01	2.5	0.1
2.5%	0.1765	5×10^{-4}	0.778	1.1877	0.0046	1.9605	3.888×10^{-23}
25%	0.2195	9×10^{-4}	0.9157	1.2478	0.0078	2.3179	9.41×10^{-18}
50%	0.2413	0.0012	0.993	1.2867	0.0105	2.5821	0.0879
75%	0.2635	0.0015	1.0732	1.3287	0.0144	2.9665	0.2113
97.5%	0.3086	0.0025	1.2198	1.418	0.0308	4.6803	0.4219
Mean	0.2415	0.0012	0.9959	1.2918	0.0125	2.7715	0.1225
Std	0.0334	5×10^{-4}	0.1144	0.0603	0.0086	0.8467	0.1305
W	0.99839	0.93256	0.99805	0.98527	0.65168	0.67378	0.86366
p -value	0.4838	$< 2.2 \times 10^{-16}$	0.306	1.696×10^{-8}	$< 2.2 \times 10^{-16}$	$< 2.2 \times 10^{-16}$	$< 2.2 \times 10^{-16}$
Mean of $\hat{\sigma}$	0.0353	0.0977	0.0294	0.0117	0.1182	0.0525	13605665162
Std of $\hat{\sigma}$	0.0033	0.0110	0.0061	0.0020	0.0285	0.0268	155951812811
Number of $\hat{\sigma}_\gamma > 10$	312						

Table A.8: Case 8

	A	c	α	p	D	q	γ
Target value	0.25	0.001	1	1.25	0.01	2.5	0.15
2.5%	0.1773	5×10^{-4}	0.7628	1.1879	0.0046	1.9621	1.10675×10^{-22}
25%	0.2211	9×10^{-4}	0.9173	1.2498	0.008	2.3098	0.01983
50%	0.2411	0.0012	1.0034	1.2862	0.0109	2.6112	0.1426
75%	0.2643	0.0016	1.0746	1.3238	0.0151	3.034	0.2597
97.5%	0.3094	0.0024	1.2294	1.4189	0.0334	4.7263	0.4915
Mean	0.2424	0.0013	0.9968	1.2896	0.0129	2.7979	0.1641
Std	0.0336	5×10^{-4}	0.1187	0.058	0.0084	0.8666	0.1495
W	0.99717	0.9578	0.99752	0.98814	0.71566	0.67839	0.91122
p -value	0.07565	$< 2.2 \times 10^{-16}$	0.1329	3.119×10^{-7}	$< 2.2 \times 10^{-16}$	$< 2.2 \times 10^{-16}$	$< 2.2 \times 10^{-16}$
Mean of $\hat{\sigma}$	0.0354	0.0982	0.0295	0.0117	0.1199	0.0535	21378356193
Std of $\hat{\sigma}$	0.0033	0.0107	0.0066	0.0019	0.0278	0.0263	448346805622
Number of $\hat{\sigma}_\gamma > 10$	312						

Table A.9: Case 9

	A	c	α	p	D	q	γ
Target value	0.25	0.001	1	1.25	0.01	2.5	0.2
2.5%	0.1802	5×10^{-4}	0.7531	1.19	0.0047	1.9306	2.3058×10^{-22}
25%	0.2186	9×10^{-4}	0.9123	1.2516	0.0077	2.2734	0.0794
50%	0.2414	0.0012	1.0019	1.2852	0.0104	2.5451	0.1919
75%	0.2657	0.0015	1.0788	1.3276	0.015	2.9953	0.3143
97.5%	0.3174	0.0026	1.2254	1.4266	0.0338	5.3555	0.5566
Mean	0.2435	0.0013	0.9952	1.2914	0.0126	2.7759	0.2074
Std	0.035	5×10^{-4}	0.1210	0.0596	0.0084	0.925	0.1588
W	0.99523	0.92047	0.99742	0.97825	0.70733	0.65368	0.94875
p -value	0.003206	$< 2.2 \times 10^{-16}$	0.1142	4.438×10^{-11}	$< 2.2 \times 10^{-16}$	$< 2.2 \times 10^{-16}$	$< 2.2 \times 10^{-16}$
Mean of $\hat{\sigma}$	0.0352	0.0977	0.0295	0.0117	0.1202	0.0533	29068230383
Std of $\hat{\sigma}$	0.0033	0.0104	0.0064	0.0019	0.0335	0.0322	6.4025×10^{11}
Number of $\hat{\sigma}_\gamma > 10$	149						

Table A.10: Case 10

	A	c	α	p	D	q	γ
Target value	0.25	0.005	1	1.25	0.001	2.5	0.1
2.5%	0.1781	0.0026	0.7612	1.194	5×10^{-4}	2.0015	3.7395×10^{-23}
25%	0.2173	0.0045	0.9275	1.2547	8×10^{-4}	2.3364	1.0175×10^{-17}
50%	0.2389	0.0058	1.0046	1.2858	0.001	2.5715	0.0941
75%	0.2632	0.0075	1.0851	1.3261	0.0014	2.9305	0.2034
97.5%	0.3054	0.013	1.2367	1.4266	0.0033	4.7497	0.429
Mean	0.2403	0.0063	1.0026	1.2924	0.0013	2.7848	0.1204
Std	0.0333	0.0026	0.1188	0.0585	9×10^{-4}	0.921	0.1267
W	0.99817	0.92158	0.9974	0.97624	0.59071	0.58092	0.86641
p -value	0.3621	$< 2.2 \times 10^{-16}$	0.1095	1.018×10^{-11}	$< 2.2 \times 10^{-16}$	$< 2.2 \times 10^{-16}$	$< 2.2 \times 10^{-16}$
Mean of $\hat{\sigma}$	0.0349	0.0976	0.0291	0.0116	0.1131	0.0499	42714516523
Std of $\hat{\sigma}$	0.0033	0.0110	0.0065	0.0018	0.0286	0.0273	6.8393×10^{11}
Number of $\hat{\sigma}_\gamma > 10$	149						

Table A.11: Case 11

	A	c	α	p	D	q	γ
Target value	0.25	0.005	1	1.25	0.001	2.5	0.15
2.5%	0.1767	0.0028	0.7511	1.1923	5×10^{-4}	1.978	1.4773×10^{-22}
25%	0.2182	0.0046	0.9231	1.2534	8×10^{-4}	2.2782	0.0357
50%	0.2395	0.0059	0.9945	1.2877	0.001	2.5736	0.1540
75%	0.2619	0.0076	1.0755	1.3266	0.0014	2.9599	0.2640
97.5%	0.3109	0.013	1.2196	1.4199	0.0033	4.9545	0.4648
Mean	0.2408	0.0064	0.9959	1.293	0.0012	2.7626	0.1667
Std	0.0335	0.0026	0.1198	0.0576	8×10^{-4}	0.8732	0.1411
W	0.9959	0.92048	0.99664	0.98054	0.65143	0.64948	0.92903
p -value	0.009382	$< 2.2 \times 10^{-16}$	0.03132	2.667×10^{-10}	$< 2.2 \times 10^{-16}$	$< 2.2 \times 10^{-16}$	$< 2.2 \times 10^{-16}$
Mean of $\hat{\sigma}$	0.0349	0.0978	0.0293	0.0117	0.1152	0.0506	7285108672
Std of $\hat{\sigma}$	0.0031	0.0105	0.0067	0.0018	0.0307	0.0292	123729085558
Number of $\hat{\sigma}_\gamma > 10$	198						

Table A.12: Case 12

	A	c	α	p	D	q	γ
Target value	0.25	0.005	1	1.25	0.001	2.5	0.2
2.5%	0.1764	0.0027	0.7717	1.1908	5×10^{-4}	1.9822	1.029×10^{-21}
25%	0.2168	0.0046	0.9285	1.2539	8×10^{-4}	2.3499	0.0738
50%	0.239	0.0059	1.0046	1.2888	0.0011	2.5853	0.2004
75%	0.2615	0.0078	1.0776	1.3298	0.0015	2.9664	0.3173
97.5%	0.2983	0.0128	1.2359	1.4276	0.0036	5.3554	0.5374
Mean	0.2386	0.0064	1.0038	1.295	0.0013	2.8158	0.2085
Std	0.0324	0.0027	0.1155	0.0597	9×10^{-4}	0.9487	0.1585
W	0.99814	0.89488	0.99682	0.97794	0.61308	0.62151	0.95155
p -value	0.3464	$< 2.2 \times 10^{-16}$	0.04233	3.512×10^{-11}	$< 2.2 \times 10^{-16}$	$< 2.2 \times 10^{-16}$	$< 2.2 \times 10^{-16}$
Mean of $\hat{\sigma}$	0.0351	0.0979	0.029	0.0117	0.1159	0.0515	4438568515
Std of $\hat{\sigma}$	0.0032	0.0105	0.0062	0.0018	0.0317	0.0306	61465795105
Number of $\hat{\sigma}_\gamma > 10$	145						

Table A.13: Case 13

	A	c	α	p	D	q	γ
Target value	0.25	0.005	1	1.25	0.005	2.5	0.1
2.5%	0.1724	0.0027	0.7383	1.1916	0.0023	1.9212	4.8638×10^{-23}
25%	0.2154	0.0047	0.9199	1.2611	0.004	2.2923	1.17×10^{-17}
50%	0.2379	0.0065	1.001	1.3031	0.0052	2.5766	0.0793
75%	0.2603	0.0082	1.0802	1.3477	0.0074	3.0132	0.1951
97.5%	0.3089	0.0133	1.233	1.4543	0.015	4.8457	0.4481
Mean	0.2388	0.0067	0.9977	1.3077	0.0063	2.7769	0.1191
Std	0.0342	0.0027	0.1227	0.068	0.0041	0.8438	0.134
W	0.99818	0.94976	0.99671	0.98273	0.66676	0.70619	0.84301
p -value	0.3652	$< 2.2 \times 10^{-16}$	0.03538	1.673×10^{-9}	$< 2.2 \times 10^{-16}$	$< 2.2 \times 10^{-16}$	$< 2.2 \times 10^{-16}$
Mean of $\hat{\sigma}$	0.0367	0.1004	0.0299	0.0132	0.1208	0.0543	4741693232
Std of $\hat{\sigma}$	0.0038	0.0113	0.0067	0.0022	0.0314	0.0290	40749325303
Number of $\hat{\sigma}_\gamma > 10$	338						

Table A.14: Case 14

	A	c	α	p	D	q	γ
Target value	0.25	0.005	1	1.25	0.005	2.5	0.15
2.5%	0.172	0.0028	0.7429	1.1974	0.0023	1.933	9.6668×10^{-23}
25%	0.214	0.0048	0.9216	1.2608	0.004	2.2982	0.0182
50%	0.2356	0.0062	1.0049	1.3037	0.0054	2.6128	0.1469
75%	0.2587	0.008	1.0793	1.3525	0.0076	3.0356	0.2512
97.5%	0.3035	0.0135	1.2308	1.4558	0.0204	5.3615	0.4593
Mean	0.2368	0.0067	0.9988	1.3098	0.0067	2.8541	0.1587
Std	0.0334	0.0029	0.1211	0.0689	0.0057	1.1276	0.1397
W	0.99806	0.86675	0.99666	0.97859	0.54753	0.56054	0.92001
p -value	0.3077	$< 2.2 \times 10^{-16}$	0.03251	5.733×10^{-11}	$< 2.2 \times 10^{-16}$	$< 2.2 \times 10^{-16}$	$< 2.2 \times 10^{-16}$
Mean of $\hat{\sigma}$	0.0369	0.1012	0.03	0.0134	0.1242	0.0571	6601357031
Std of $\hat{\sigma}$	0.0039	0.0116	0.0069	0.0026	0.0408	0.0398	67373198841
Number of $\hat{\sigma}_\gamma > 10$	219						

Table A.15: Case 15

	A	c	α	p	D	q	γ
Target value	0.25	0.005	1	1.25	0.005	2.5	0.2
2.5%	0.1701	0.0028	0.739	1.1987	0.0023	1.9318	5.6155×10^{-22}
25%	0.2143	0.0049	0.9099	1.2645	0.0039	2.2651	0.0562
50%	0.2372	0.0064	0.9915	1.3059	0.0054	2.5787	0.1807
75%	0.261	0.0083	1.0688	1.3537	0.0073	2.9649	0.2979
97.5%	0.3048	0.0134	1.2328	1.4613	0.0178	5.0659	0.5240
Mean	0.2382	0.0069	0.9896	1.3129	0.0064	2.7765	0.1965
Std	0.0345	0.0028	0.119	0.0691	0.0044	0.9298	0.1592
W	0.99861	0.93664	0.99843	0.97494	0.68134	0.64855	0.93918
p -value	0.6258	$< 2.2 \times 10^{-16}$	0.5127	4.073×10^{-12}	$< 2.2 \times 10^{-16}$	$< 2.2 \times 10^{-16}$	$< 2.2 \times 10^{-16}$
Mean of $\hat{\sigma}$	0.0366	0.101	0.0301	0.0135	0.1226	0.0546	9110180630
Std of $\hat{\sigma}$	0.0037	0.0114	0.0066	0.0023	0.0329	0.0316	174709931464
Number of $\hat{\sigma}_\gamma > 10$	165						

Table A.16: Case 16

	A	c	α	p	D	q	γ
Target value	0.25	0.005	1	1.25	0.01	2.5	0.1
2.5%	0.1716	0.0028	0.7611	1.2014	0.0046	1.9105	3.6498×10^{-23}
25%	0.2119	0.0048	0.9196	1.2667	0.0079	2.3073	1.6725×10^{-17}
50%	0.2321	0.0063	1.0041	1.3082	0.0109	2.6502	0.0910
75%	0.257	0.0083	1.0853	1.3546	0.0159	3.115	0.2136
97.5%	0.3041	0.0136	1.2212	1.4831	0.0436	5.9823	0.4402
Mean	0.2342	0.0069	1.0014	1.3159	0.0143	2.9696	0.1262
Std	0.0337	0.0029	0.1207	0.0712	0.0199	1.7732	0.1375
W	0.99628	0.92826	0.99681	0.97162	0.28335	0.36042	0.85416
p -value	0.01729	$< 2.2 \times 10^{-16}$	0.0418	4.533×10^{-13}	$< 2.2 \times 10^{-16}$	$< 2.2 \times 10^{-16}$	$< 2.2 \times 10^{-16}$
Mean of $\hat{\sigma}$	0.0378	0.1033	0.0303	0.0142	0.1317	0.0623	14601363856
Std of $\hat{\sigma}$	0.0038	0.0110	0.0069	0.0025	0.0416	0.0403	266858479911
Number of $\hat{\sigma}_\gamma > 10$	327						

Table A.17: Case 17

	A	c	α	p	D	q	γ
Target value	0.25	0.005	1	1.25	0.01	2.5	0.15
2.5%	0.1737	0.0028	0.7411	1.2003	0.0042	1.8788	2.7875×10^{-22}
25%	0.2154	0.0049	0.9156	1.2673	0.0077	2.2481	0.0133
50%	0.2358	0.0064	0.9918	1.3102	0.0102	2.5322	0.1357
75%	0.2596	0.0084	1.0734	1.3545	0.0146	3.0057	0.26
97.5%	0.3112	0.0139	1.2058	1.4737	0.0334	4.9858	0.5248
Mean	0.2383	0.0069	0.9894	1.3162	0.0126	2.7734	0.1642
Std	0.0353	0.0029	0.1204	0.0711	0.0094	0.9334	0.1517
W	0.99479	0.9314	0.99459	0.95938	0.64662	0.68558	0.90729
p -value	0.001417	$< 2.2 \times 10^{-16}$	0.001052	3.426×10^{-16}	$< 2.2 \times 10^{-16}$	$< 2.2 \times 10^{-16}$	$< 2.2 \times 10^{-16}$
Mean of $\hat{\sigma}$	0.0375	0.1024	0.0306	0.0142	0.1265	0.0572	12601151375
Std of $\hat{\sigma}$	0.0037	0.0113	0.0070	0.0026	0.0320	0.0312	230088375740
Number of $\hat{\sigma}_\gamma > 10$	245						

Table A.18: Case 18

	A	c	α	p	D	q	γ
Target value	0.25	0.005	1	1.25	0.01	2.5	0.2
2.5%	0.172	0.003	0.7574	1.1982	0.0044	1.8924	1.4763×10^{-21}
25%	0.2126	0.0049	0.911	1.2702	0.0078	2.2808	0.0543
50%	0.237	0.0064	0.9953	1.3107	0.0105	2.5653	0.1806
75%	0.259	0.0083	1.0769	1.3608	0.0152	3.0289	0.3184
97.5%	0.3051	0.0159	1.2302	1.4931	0.0372	5.0654	0.5433
Mean	0.2365	0.0071	0.9931	1.3211	0.0128	2.7928	0.1994
Std	0.035	0.0032	0.122	0.0771	0.0088	0.8765	0.1621
W	0.99829	0.88083	0.99866	0.94191	0.7212	0.75927	0.93815
p -value	0.4257	$< 2.2 \times 10^{-16}$	0.6614	$< 2.2 \times 10^{-16}$			
Mean of $\hat{\sigma}$	0.0377	0.1029	0.0306	0.0144	0.1283	0.0581	10190614485
Std of $\hat{\sigma}$	0.0040	0.0118	0.0070	0.0028	0.0292	0.0284	153910761896
Number of $\hat{\sigma}_\gamma > 10$	181						

Table A.19: Case 19

	A	c	α	p	D	q	γ
Target value	0.25	0.01	1	1.25	0.001	2.5	0.1
2.5%	0.173	0.0053	0.7688	1.1953	5×10^{-4}	1.9409	2.5525×10^{-23}
25%	0.2143	0.0092	0.9328	1.2551	8×10^{-4}	2.28	4.4425×10^{-17}
50%	0.2375	0.0119	1.0065	1.2943	0.001	2.5551	0.0902
75%	0.2593	0.0152	1.0837	1.3392	0.0014	2.9354	0.2161
97.5%	0.3	0.0262	1.2322	1.4612	0.0033	4.9831	0.4511
Mean	0.2369	0.0128	1.0083	1.3003	0.0012	2.7753	0.1289781
Std	0.0337	0.0053	0.1167	0.0647	0.001	1.0377	0.1366
W	0.99903	0.91705	0.99863	0.97837	0.56276	0.54308	0.86598
p -value	0.8874	$< 2.2 \times 10^{-16}$	0.6403	4.866×10^{-11}	$< 2.2 \times 10^{-16}$	$< 2.2 \times 10^{-16}$	$< 2.2 \times 10^{-16}$
Mean of $\hat{\sigma}$	0.0359	0.0996	0.0292	0.0125	0.1189	0.0536	20686130382
Std of $\hat{\sigma}$	0.0037	0.0117	0.0063	0.0020	0.0496	0.0474	317962206389
Number of $\hat{\sigma}_\gamma > 10$	305						

Table A.20: Case 20

	A	c	α	p	D	q	γ
Target value	0.25	0.01	1	1.25	0.001	2.5	0.15
2.5%	0.1744	0.0055	0.7676	1.1919	5×10^{-4}	1.9594	2.139×10^{-22}
25%	0.2139	0.0091	0.9296	1.2566	8×10^{-4}	2.3247	0.0248
50%	0.2342	0.0118	1.0124	1.2939	0.0011	2.6038	0.1397
75%	0.2587	0.016	1.086	1.3384	0.0015	2.9808	0.2649
97.5%	0.3051	0.0292	1.2239	1.4559	0.0033	4.8827	0.4758
Mean	0.2367	0.0132	1.0067	1.3024	0.0013	2.823	0.1634
Std	0.0338	0.006	0.1202	0.0663	0.0011	1.1845	0.147
W	0.99537	0.88538	0.99788	0.9659	0.4779	0.45543	0.91456
p -value	0.003981	$< 2.2 \times 10^{-16}$	0.2374	1.495×10^{-14}	$< 2.2 \times 10^{-16}$	$< 2.2 \times 10^{-16}$	$< 2.2 \times 10^{-16}$
Mean of $\hat{\sigma}$	0.036	0.0999	0.0292	0.0126	0.1191	0.0537	5601037538
Std of $\hat{\sigma}$	0.0035	0.0111	0.0066	0.0021	0.0408	0.0395	98440638759
Number of $\hat{\sigma}_\gamma > 10$	212						

Table A.21: Case 21

	A	c	α	p	D	q	γ
Target value	0.25	0.01	1	1.25	0.001	2.5	0.2
2.5%	0.1681	0.0057	0.7649	1.194	5×10^{-4}	1.9673	2.362×10^{-21}
25%	0.2134	0.0094	0.9285	1.2601	8×10^{-4}	2.2843	0.0714
50%	0.2379	0.0123	0.9956	1.3003	0.001	2.5772	0.1983
75%	0.2608	0.0159	1.0744	1.3423	0.0015	2.9693	0.313
97.5%	0.3083	0.0262	1.2335	1.4441	0.0035	5.1072	0.5362
Mean	0.2378	0.0134	1.0012	1.3051	0.0013	2.7864	0.2075
Std	0.035	0.0058	0.117	0.0653	8×10^{-4}	0.9212	0.159
W	0.99895	0.88409	0.99403	0.96044	0.69848	0.6587	0.95035
p -value	0.8445	$< 2.2 \times 10^{-16}$	0.0005167	8.18×10^{-16}	$< 2.2 \times 10^{-16}$	$< 2.2 \times 10^{-16}$	$< 2.2 \times 10^{-16}$
Mean of $\hat{\sigma}$	0.0359	0.1004	0.0296	0.0128	0.1188	0.0528	1210379274
Std of $\hat{\sigma}$	0.0036	0.0116	0.0064	0.0022	0.0314	0.0299	12056890816
Number of $\hat{\sigma}_\gamma > 10$	137						

Table A.22: Case 22

	A	c	α	p	D	q	γ
Target value	0.25	0.01	1	1.25	0.005	2.5	0.1
2.5%	0.17	0.0055	0.7608	1.2003	0.0025	1.9499	3.2468×10^{-23}
25%	0.2088	0.0097	0.9245	1.2666	0.0039	2.3134	8.395×10^{-18}
50%	0.2315	0.013	0.9994	1.3149	0.0053	2.5918	0.0775
75%	0.2531	0.0177	1.0904	1.3698	0.0074	3.0475	0.2048
97.5%	0.3059	0.0305	1.222	1.504	0.0165	5.2881	0.4468
Mean	0.2325	0.0143	1.0015	1.3227	0.0064	2.8275	0.1221
Std	0.0342	0.0065	0.1205	0.0771	0.0041	0.8875	0.1373
W	0.99586	0.91887	0.99596	0.97649	0.72212	0.72611	0.84453
p -value	0.008731	$< 2.2 \times 10^{-16}$	0.01034	1.215×10^{-11}	$< 2.2 \times 10^{-16}$	$< 2.2 \times 10^{-16}$	$< 2.2 \times 10^{-16}$
Mean of $\hat{\sigma}$	0.0381	0.1042	0.0304	0.0147	0.1272	0.0587	13727565619
Std of $\hat{\sigma}$	0.0039	0.0120	0.0070	0.0027	0.0320	0.0305	171710279884
Number of $\hat{\sigma}_\gamma > 10$	334						

Table A.23: Case 23

	A	c	α	p	D	q	γ
Target value	0.25	0.01	1	1.25	0.005	2.5	0.15
2.5%	0.1731	0.0054	0.7399	1.1979	0.0023	1.9278	3.348×10^{-22}
25%	0.2135	0.0098	0.9196	1.2715	0.004	2.3041	3.5975×10^{-15}
50%	0.2348	0.0129	0.9871	1.3136	0.0055	2.6216	0.1367312
75%	0.2563	0.0169	1.063	1.3601	0.0078	3.0832	0.2622592
97.5%	0.304	0.0281	1.2152	1.5071	0.0172	5.053	0.5008
Mean	0.2355	0.014	0.9885	1.3222	0.0066	2.8445	0.1614346
Std	0.0338	0.0063	0.119	0.0767	0.0048	0.9893	0.1524
W	0.99651	0.89021	0.99319	0.95127	0.62384	0.65579	0.90175
p -value	0.02518	$< 2.2 \times 10^{-16}$	0.000154	$< 2.2 \times 10^{-16}$			
Mean of $\hat{\sigma}$	0.0379	0.1042	0.0309	0.0147	0.131	0.0622	3340203824
Std of $\hat{\sigma}$	0.0039	0.0121	0.0076	0.0027	0.0727	0.0723	55586874625
Number of $\hat{\sigma}_\gamma > 10$	264						

Table A.24: Case 24

	A	c	α	p	D	q	γ
Target value	0.25	0.01	1	1.25	0.005	2.5	0.2
2.5%	0.1704	0.006	0.7471	1.2026	0.0022	1.9298	9.9918×10^{-22}
25%	0.211	0.0098	0.9101	1.2727	0.0039	2.2868	0.0622
50%	0.2331	0.0131	0.9988	1.3173	0.0053	2.5564	0.1939
75%	0.256	0.0173	1.0749	1.3678	0.0076	3.0109	0.3138
97.5%	0.3031	0.0309	1.2275	1.4956	0.0186	5.5108	0.5678
Mean	0.2343	0.0144	0.9919	1.3255	0.0065	2.8393	0.2052
Std	0.0347	0.0066	0.122	0.0771	0.0049	1.1235	0.1646
W	0.99701	0.89515	0.99848	0.96905	0.64367	0.58172	0.94124
p -value	0.05816	$< 2.2 \times 10^{-16}$	0.5424	9.327×10^{-14}	$< 2.2 \times 10^{-16}$	$< 2.2 \times 10^{-16}$	$< 2.2 \times 10^{-16}$
Mean of $\hat{\sigma}$	0.0381	0.1045	0.0309	0.0149	0.129	0.0595	22297421807
Std of $\hat{\sigma}$	0.0041	0.0119	0.0070	0.0028	0.0418	0.0410	4.2881×10^{11}
Number of $\hat{\sigma}_\gamma > 10$	171						

Table A.25: Case 25

	A	c	α	p	D	q	γ
Target value	0.25	0.01	1	1.25	0.01	2.5	0.1
2.5%	0.1641	0.0062	0.7565	1.201	0.0048	1.9353	4.837×10^{-23}
25%	0.2077	0.0103	0.9248	1.28	0.008	2.3073	5.54×10^{-18}
50%	0.2296	0.0133	1.0073	1.3234	0.011	2.6219	0.0831
75%	0.2556	0.0177	1.0839	1.3811	0.0154	3.1307	0.2133
97.5%	0.305	0.031	1.2465	1.5179	0.0377	5.2652	0.4426
Mean	0.2313	0.0148	1.0053	1.3352	0.0135	2.9007	0.1244
Std	0.0356	0.0066	0.1227	0.0811	0.01	1.1036	0.136
W	0.99812	0.90153	0.99778	0.96105	0.65581	0.64381	0.85454
p -value	0.3256	$< 2.2 \times 10^{-16}$	0.1947	8.538×10^{-16}	$< 2.2 \times 10^{-16}$	$< 2.2 \times 10^{-16}$	$< 2.2 \times 10^{-16}$
Mean of $\hat{\sigma}$	0.039	0.105	0.0306	0.0157	0.1361	0.066	12458750513
Std of $\hat{\sigma}$	0.0042	0.0118	0.0070	0.0031	0.0588	0.0580	139724100630
Number of $\hat{\sigma}_\gamma > 10$	342						

Table A.26: Case 26

	A	c	α	p	D	q	γ
Target value	0.25	0.01	1	1.25	0.01	2.5	0.15
2.5%	0.1666	0.0058	0.7265	1.203	0.0041	1.8517	2.28×10^{-22}
25%	0.2073	0.0102	0.9183	1.2839	0.0076	2.2777	8.6075×10^{-16}
50%	0.2298	0.0134	1.0008	1.3294	0.0107	2.593	0.1282
75%	0.2544	0.0181	1.073	1.386	0.0154	3.0237	0.2498
97.5%	0.3048	0.0308	1.2372	1.5336	0.039	5.5144	0.4603
Mean	0.2315	0.0146	0.9931	1.3389	0.0131	2.829	0.1515
Std	0.0351	0.0064	0.1243	0.0816	0.0094	0.985	0.1435
W	0.99523	0.93077	0.99356	0.9706	0.71488	0.7088	0.90016
p -value	0.003206	$< 2.2 \times 10^{-16}$	0.0002608	2.393×10^{-13}	$< 2.2 \times 10^{-16}$	$< 2.2 \times 10^{-16}$	$< 2.2 \times 10^{-16}$
Mean of $\hat{\sigma}$	0.0389	0.1054	0.0312	0.0159	0.1343	0.0627	6207769583
Std of $\hat{\sigma}$	0.0042	0.0116	0.0077	0.0031	0.0385	0.0369	75094278693
Number of $\hat{\sigma}_\gamma > 10$	275						

Table A.27: Case 27

	A	c	α	p	D	q	γ
Target value	0.25	0.01	1	1.25	0.01	2.5	0.2
2.5%	0.1677	0.0058	0.7357	1.2055	0.0042	1.8622	5.871×10^{-22}
25%	0.2087	0.01	0.9121	1.2803	0.008	2.2866	0.0323
50%	0.2314	0.0135	0.9918	1.3271	0.0109	2.6032	0.1681
75%	0.2537	0.0176	1.0767	1.3849	0.0156	3.0843	0.3040
97.5%	0.3043	0.03	1.2207	1.5076	0.0414	5.5123	0.5511
Mean	0.2326	0.0144	0.9909	1.3354	0.0139	2.8946	0.1886
Std	0.0347	0.0062	0.1237	0.081	0.0116	1.1753	0.1645
W	0.99604	0.91837	0.99607	0.97039	0.60906	0.62947	0.922
p -value	0.01165	$< 2.2 \times 10^{-16}$	0.01232	2.102×10^{-13}	$< 2.2 \times 10^{-16}$	$< 2.2 \times 10^{-16}$	$< 2.2 \times 10^{-16}$
Mean of $\hat{\sigma}$	0.039	0.1057	0.0313	0.0158	0.1363	0.0647	2447544332
Std of $\hat{\sigma}$	0.0040	0.0117	0.0074	0.0029	0.0433	0.0426	30620164505
Number of $\hat{\sigma}_\gamma > 10$	198						

Appendix B

Table B.1: Estimates of the ETAS model parameters, and the corresponding end of the study time interval.

Ending time	$\hat{\nu}$	\hat{A}	\hat{c}	$\hat{\alpha}$	\hat{p}	\hat{D}	\hat{q}	$\hat{\gamma}$
2018/10/21 00:00:00	0.663	0.240	0.007	0.987	1.217	0.003	2.479	0.170
2018/10/21 12:00:00	0.663	0.240	0.007	0.987	1.218	0.003	2.477	0.172
2018/10/22 00:00:00	0.663	0.238	0.007	0.990	1.218	0.003	2.481	0.175
2018/10/22 12:00:00	0.667	0.212	0.013	1.186	1.295	0.001	1.736	0.542
2018/10/23 00:00:00	0.666	0.215	0.012	1.177	1.297	0.001	1.773	0.506
2018/10/23 12:00:00	0.666	0.213	0.013	1.190	1.294	0.001	1.775	0.467
2018/10/24 00:00:00	0.668	0.228	0.014	1.182	1.289	0.001	1.724	0.450
2018/10/24 12:00:00	0.666	0.239	0.013	1.153	1.284	0.001	1.739	0.423
2018/10/25 00:00:00	0.667	0.238	0.013	1.156	1.284	0.001	1.742	0.425
2018/10/25 12:00:00	0.668	0.237	0.013	1.164	1.282	0.001	1.748	0.417
2018/10/26 00:00:00	0.667	0.238	0.013	1.174	1.275	0.001	1.722	0.442
2018/10/26 12:00:00	0.669	0.251	0.013	1.158	1.275	0.001	1.656	0.433
2018/10/27 00:00:00	0.669	0.252	0.014	1.156	1.276	0.001	1.633	0.422
2018/10/27 12:00:00	0.667	0.250	0.013	1.157	1.278	0.001	1.641	0.416
2018/10/28 00:00:00	0.669	0.254	0.013	1.150	1.275	0.001	1.631	0.410
2018/10/28 12:00:00	0.670	0.254	0.013	1.150	1.273	0.001	1.646	0.400

Ending time	$\hat{\nu}$	\hat{A}	\hat{c}	$\hat{\alpha}$	\hat{p}	\hat{D}	\hat{q}	$\hat{\gamma}$
2018/10/29 00:000	0.669	0.254	0.013	1.151	1.273	0.001	1.641	0.404
2018/10/29 12:000	0.669	0.259	0.013	1.138	1.271	0.001	1.655	0.388
2018/10/30 00:000	0.669	0.258	0.013	1.139	1.272	0.001	1.649	0.392
2018/10/30 12:000	0.669	0.260	0.013	1.141	1.267	0.001	1.641	0.399
2018/10/31 00:000	0.668	0.259	0.013	1.141	1.268	0.001	1.644	0.394
2018/10/31 12:000	0.670	0.257	0.013	1.143	1.271	0.001	1.644	0.393
2018/11/01 00:000	0.669	0.259	0.013	1.139	1.271	0.001	1.644	0.391
2018/11/01 12:000	0.669	0.258	0.014	1.151	1.264	0.001	1.652	0.385
2018/11/02 00:000	0.669	0.258	0.013	1.151	1.265	0.001	1.651	0.384
2018/11/02 12:000	0.669	0.257	0.013	1.151	1.265	0.001	1.656	0.383
2018/11/03 00:000	0.669	0.257	0.013	1.150	1.266	0.001	1.651	0.381
2018/11/03 12:000	0.671	0.256	0.014	1.151	1.267	0.001	1.650	0.385
2018/11/04 00:000	0.669	0.256	0.014	1.149	1.267	0.001	1.652	0.385
2018/11/04 12:000	0.671	0.255	0.014	1.150	1.270	0.001	1.650	0.381
2018/11/05 00:000	0.670	0.255	0.014	1.151	1.269	0.001	1.651	0.384
2018/11/05 12:000	0.669	0.256	0.014	1.148	1.269	0.001	1.652	0.383
2018/11/06 00:000	0.669	0.256	0.013	1.153	1.263	0.001	1.650	0.370
2018/11/06 12:000	0.669	0.256	0.013	1.153	1.263	0.001	1.642	0.373
2018/11/07 00:000	0.670	0.254	0.013	1.155	1.265	0.001	1.650	0.374
2018/11/07 12:000	0.670	0.254	0.013	1.156	1.265	0.001	1.650	0.374
2018/11/08 00:000	0.669	0.256	0.013	1.151	1.265	0.001	1.645	0.372
2018/11/08 12:000	0.669	0.255	0.013	1.151	1.265	0.001	1.644	0.371
2018/11/09 00:000	0.669	0.255	0.014	1.152	1.267	0.001	1.649	0.370
2018/11/09 12:000	0.670	0.253	0.014	1.154	1.268	0.001	1.652	0.374
2018/11/10 00:000	0.669	0.255	0.014	1.151	1.268	0.001	1.645	0.374
2018/11/10 12:000	0.669	0.254	0.014	1.151	1.268	0.001	1.647	0.375
2018/11/11 00:000	0.670	0.253	0.014	1.154	1.269	0.001	1.645	0.374

Ending time	$\hat{\nu}$	\hat{A}	\hat{c}	$\hat{\alpha}$	\hat{p}	\hat{D}	\hat{q}	$\hat{\gamma}$
2018/11/11 12:000	0.669	0.254	0.014	1.150	1.270	0.001	1.645	0.369
2018/11/12 00:000	0.671	0.253	0.014	1.152	1.270	0.001	1.646	0.372
2018/11/12 12:000	0.669	0.254	0.014	1.150	1.270	0.001	1.641	0.376
2018/11/13 00:000	0.669	0.254	0.014	1.148	1.271	0.001	1.647	0.368
2018/11/13 12:000	0.669	0.254	0.014	1.148	1.271	0.001	1.650	0.364
2018/11/14 00:000	0.668	0.254	0.014	1.149	1.271	0.001	1.650	0.371
2018/11/14 12:000	0.669	0.254	0.014	1.148	1.272	0.001	1.647	0.369
2018/11/15 00:000	0.668	0.254	0.014	1.148	1.272	0.001	1.650	0.366
2018/11/15 12:000	0.668	0.253	0.014	1.150	1.272	0.001	1.645	0.373
2018/11/16 00:000	0.669	0.254	0.014	1.147	1.273	0.001	1.651	0.365
2018/11/16 12:000	0.668	0.254	0.013	1.157	1.265	0.001	1.650	0.366
2018/11/17 00:000	0.670	0.252	0.013	1.160	1.265	0.001	1.652	0.372
2018/11/17 12:000	0.669	0.254	0.013	1.157	1.265	0.001	1.647	0.369
2018/11/18 00:00:00	0.670	0.254	0.014	1.156	1.266	0.001	1.646	0.367
2018/11/18 12:00:00	0.669	0.253	0.014	1.157	1.267	0.001	1.648	0.371
2018/11/19 00:00:00	0.668	0.252	0.014	1.158	1.268	0.001	1.649	0.372
2018/11/19 12:00:00	0.668	0.253	0.014	1.156	1.266	0.001	1.653	0.369
2018/11/20 00:00:00	0.670	0.251	0.014	1.159	1.268	0.001	1.653	0.370
2018/11/20 12:00:00	0.670	0.251	0.014	1.158	1.269	0.001	1.653	0.366

Appendix C

Table C.1: Asymptotic standard errors for the estimators of seven parameters of the ETAS model obtained with 40 Monte Carlo simulations using the parameter values reported in Table 2.1 as targets, and their mean value for each parameter.

	A	c	α	p	D	q	γ
1	0.0408	0.1062	0.0234	0.0114	0.1353	0.0730	0.1910
2	0.0348	0.0959	0.0303	0.0144	0.1032	0.0470	946158694.0600
3	0.0380	0.1039	0.0258	0.0121	0.1155	0.0262	0.2032
4	0.0392	0.1108	0.0310	0.0125	0.1213	0.0466	0.3473
5	0.0457	0.1191	0.0364	0.0180	0.1634	0.0686	25403780640.9007
6	0.0384	0.1117	0.0231	0.0133	0.1563	0.0911	0.0607
7	0.0408	0.1052	0.0200	0.0131	0.1248	0.0679	39694308.9377
8	0.0410	0.0990	0.0238	0.0151	0.1139	0.0493	0.0898
9	0.0379	0.1036	0.0255	0.0151	0.1260	0.0603	0.0918
10	0.0416	0.1270	0.0366	0.0154	0.1381	0.0653	390295337.4351
11	0.0418	0.0938	0.0219	0.0111	0.1008	0.0299	0.2691
12	0.0500	0.1553	0.0310	0.0210	0.1420	0.0541	1.1122
13	0.0364	0.1046	0.0283	0.0128	0.1058	0.0477	0.2020
14	0.0542	0.1230	0.0248	0.0121	0.1350	0.0607	0.1918
15	0.0389	0.1074	0.0252	0.0118	0.1145	0.0367	0.7691

	A	c	α	p	D	q	γ
16	0.0379	0.1009	0.0286	0.0138	0.1108	0.0377	47096081.6904
17	0.0435	0.1143	0.0271	0.0133	0.1264	0.0455	0.1322
18	0.0325	0.0976	0.0340	0.0131	0.1194	0.0594	0.2851
19	0.0378	0.1112	0.0363	0.0128	0.1218	0.0479	0.1857
20	0.0342	0.1111	0.0307	0.0150	0.1168	0.0453	0.0946
21	0.0459	0.1157	0.0559	0.0137	0.1273	0.0536	0.1006
22	0.0421	0.1075	0.0577	0.0122	0.1191	0.0528	1717423847.1487
23	0.0379	0.0974	0.0250	0.0135	0.1017	0.0416	0.1782
24	0.0378	0.1028	0.0260	0.0128	0.1163	0.0390	0.2119
25	0.0353	0.0990	0.0271	0.0138	0.1252	0.0529	0.0574
26	0.0402	0.1138	0.0232	0.0153	0.1172	0.0372	0.1421
27	0.0407	0.1254	0.0510	0.0146	0.1207	0.0411	0.5699
28	0.0428	0.1127	0.0365	0.0143	0.1175	0.0515	0.0810
29	0.0375	0.0911	0.0260	0.0115	0.1055	0.0432	0.3501
30	0.0364	0.1143	0.0255	0.0163	0.1094	0.0335	0.2275
31	0.0428	0.1196	0.0476	0.0129	0.1429	0.0521	0.2097
32	0.0438	0.1169	0.0279	0.0118	0.1011	0.0289	0.1934
33	0.0390	0.1100	0.0293	0.0131	0.1131	0.0286	0.1679
34	0.0378	0.1091	0.0326	0.0122	0.1140	0.0469	0.5630
35	0.0428	0.1127	0.0240	0.0132	0.0949	0.0349	5478599168.7306
36	0.0588	0.1329	0.0328	0.0115	0.1410	0.0583	0.4877
37	0.0391	0.1215	0.0285	0.0160	0.1284	0.0533	20218150844.4800
38	0.0383	0.1127	0.0246	0.0130	0.1092	0.0394	0.0845
39	0.0381	0.1098	0.0347	0.0127	0.1453	0.0763	564119550.4884
40	0.0453	0.1221	0.0272	0.0141	0.1379	0.0464	0.6624
Mean	0.0407	0.1112	0.0307	0.0136	0.1220	0.0493	1370132962.0536

Table C.2: Bootstrap standard errors for the estimators of seven parameters of the ETAS model obtained with 1000 bootstrap simulations for each of the 40 Monte Carlo simulations in Table C.1, and their mean value for each parameter.

	A	c	α	p	D	q	γ
1	0.0296	0.0055	0.1201	0.0806	10471036.5119	2874264170.3823	0.1463
2	0.0324	0.0078	0.1118	0.0834	923072.4674	199930332.0212	0.0945
3	0.0334	0.0051	0.1241	0.0711	0.0007	0.2655	0.2054
4	0.0362	0.0043	0.1232	0.0794	1361446.7307	368699010.1716	0.1541
5	0.0439	0.0117	0.2104	0.1688	359158.1503	215270782.8930	0.1359
6	0.0295	0.0055	0.1166	0.0808	43256.7508	24106792.8614	0.1560
7	0.0272	0.0062	0.1059	0.0753	1913188.0907	481032747.6321	0.0858
8	0.0270	0.0042	0.1262	0.1013	2775232.5815	1605023408.0711	0.1951
9	0.0278	0.0065	0.1174	0.0944	207061.7423	74268771.8311	0.1755
10	0.0339	0.0078	0.1414	0.0982	7024417.2642	2390797474.9694	0.1131
11	0.0316	0.0085	0.1064	0.0761	0.0014	0.3623	0.1538
12	0.0267	0.0096	0.1369	0.1296	16618308.1069	3507012694.6398	0.1440
13	0.0334	0.0063	0.1222	0.0812	58608.9587	17264840.1127	0.1624
14	0.0306	0.0035	0.1240	0.0695	2179913.7431	594990989.6612	0.1627
15	0.0327	0.0058	0.1058	0.0672	0.0049	1.6560	0.1254
16	0.0325	0.0079	0.1146	0.0852	0.0054	2.3947	0.1097
17	0.0318	0.0043	0.1411	0.0834	16020.4047	6795390.4113	0.2054
18	0.0347	0.0055	0.1377	0.0798	1183.3510	448374.6315	0.1508
19	0.0351	0.0054	0.1324	0.0796	2701.0438	791613.2227	0.1901
20	0.0309	0.0025	0.1221	0.0850	73947.2832	41542514.6503	0.1907
21	0.0394	0.0042	0.1577	0.0817	4837663.4675	1832880825.6835	0.2463
22	0.0413	0.0035	0.1525	0.0713	278169.3481	69117560.0081	0.1285
23	0.0301	0.0035	0.1189	0.0759	7738.6759	3076688.0594	0.1689

	A	c	α	p	D	q	γ
24	0.0325	0.0061	0.1160	0.0858	0.0028	0.7453	0.1679
25	0.0306	0.0040	0.1207	0.0901	3373788.9710	1560528318.6360	0.1837
26	0.0283	0.0060	0.1174	0.1018	0.0031	1.3259	0.1924
27	0.0355	0.0034	0.1548	0.0850	4168.4380	1737987.7027	0.1866
28	0.0332	0.0048	0.1290	0.0790	1357451.0473	855275483.6616	0.2116
29	0.0316	0.0027	0.1115	0.0615	0.0082	1.7677	0.1302
30	0.0319	0.0093	0.1171	0.0970	0.0014	0.5659	0.1695
31	0.0370	0.0080	0.1487	0.0918	102894.8256	70750269.0467	0.2062
32	0.0353	0.0046	0.1220	0.0685	0.0030	1.5594	0.1984
33	0.0327	0.0039	0.1268	0.0738	0.0010	0.3637	0.1981
34	0.0340	0.0043	0.1164	0.0661	7742.4898	2915153.2898	0.1246
35	0.0309	0.0050	0.1334	0.0777	4461400.2022	1243860235.0405	0.1303
36	0.0412	0.0028	0.1337	0.0613	831597.0915	185305064.1067	0.1422
37	0.0289	0.0076	0.1263	0.0958	77229508.7904	21959971320.3446	0.1006
38	0.0309	0.0043	0.1300	0.0805	1278.1098	531671.2748	0.2016
39	0.0350	0.0032	0.1245	0.0732	1668913.2557	528788713.8063	0.0972
40	0.0338	0.0069	0.1359	0.0869	0.0042	0.9052	0.1478
Mean	0.0329	0.0056	0.1283	0.0844	3454771.6983	1017924480.2666	0.1597

Table C.3: Length of the 95% asymptotic confidence intervals for seven parameters of the ETAS model, obtained with 40 Monte Carlo simulations (i.e., the same 40 Monte Carlo simulations as for Table C.1), and the mean length of these intervals for each parameter.

	A	c	α	p	D	q	γ
1	0.1599	0.4163	0.0917	0.0447	0.5304	0.2862	0.7487
2	0.1364	0.3759	0.1188	0.0564	0.4045	0.1842	3708942081
3	0.149	0.4073	0.1011	0.0474	0.4528	0.1027	0.7965

	A	c	α	p	D	q	γ
4	0.1537	0.4343	0.1215	0.049	0.4755	0.1827	1.3614
5	0.1791	0.4669	0.1427	0.0706	0.6405	0.2689	99582820113
6	0.1505	0.4379	0.0906	0.0521	0.6127	0.3571	0.2379
7	0.1599	0.4124	0.0784	0.0514	0.4892	0.2662	155601691
8	0.1607	0.3881	0.0933	0.0592	0.4465	0.1933	0.352
9	0.1486	0.4061	0.1	0.0592	0.4939	0.2364	0.3599
10	0.1631	0.4978	0.1435	0.0604	0.5414	0.256	1529957723
11	0.1639	0.3677	0.0858	0.0435	0.3951	0.1172	1.0549
12	0.196	0.6088	0.1215	0.0823	0.5566	0.2121	4.3598
13	0.1427	0.41	0.1109	0.0502	0.4147	0.187	0.7918
14	0.2125	0.4822	0.0972	0.0474	0.5292	0.2379	0.7519
15	0.1525	0.421	0.0988	0.0463	0.4488	0.1439	3.0149
16	0.1486	0.3955	0.1121	0.0541	0.4343	0.1478	184616640.2
17	0.1705	0.4481	0.1062	0.0521	0.4955	0.1784	0.5182
18	0.1274	0.3826	0.1333	0.0514	0.468	0.2328	1.1176
19	0.1482	0.4359	0.1423	0.0502	0.4775	0.1878	0.7279
20	0.1341	0.4355	0.1203	0.0588	0.4579	0.1776	0.3708
21	0.1799	0.4535	0.2191	0.0537	0.499	0.2101	0.3944
22	0.165	0.4214	0.2262	0.0478	0.4669	0.207	6732301480
23	0.1486	0.3818	0.098	0.0529	0.3987	0.1631	0.6985
24	0.1482	0.403	0.1019	0.0502	0.4559	0.1529	0.8306
25	0.1384	0.3881	0.1062	0.0541	0.4908	0.2074	0.225
26	0.1576	0.4461	0.0909	0.06	0.4594	0.1458	0.557
27	0.1595	0.4916	0.1999	0.0572	0.4731	0.1611	2.234
28	0.1678	0.4418	0.1431	0.0561	0.4606	0.2019	0.3175
29	0.147	0.3571	0.1019	0.0451	0.4136	0.1693	1.3724
30	0.1427	0.4481	0.1	0.0639	0.4288	0.1313	0.8918

	A	c	α	p	D	q	γ
31	0.1678	0.4688	0.1866	0.0506	0.5602	0.2042	0.822
32	0.1717	0.4582	0.1094	0.0463	0.3963	0.1133	0.7581
33	0.1529	0.4312	0.1149	0.0514	0.4434	0.1121	0.6582
34	0.1482	0.4277	0.1278	0.0478	0.4469	0.1838	2.207
35	0.1678	0.4418	0.0941	0.0517	0.372	0.1368	21476108742
36	0.2305	0.521	0.1286	0.0451	0.5527	0.2285	1.9118
37	0.1533	0.4763	0.1117	0.0627	0.5033	0.2089	79255151308
38	0.1501	0.4418	0.0964	0.051	0.4281	0.1544	0.3312
39	0.1494	0.4304	0.136	0.0498	0.5696	0.2991	2211348638
40	0.1776	0.4786	0.1066	0.0553	0.5406	0.1819	2.5966
Mean	0.1595	0.436	0.1202	0.0535	0.4781	0.1932	5370921211

Table C.4: Length of the 95% bootstrap confidence intervals (derived from the 2.5% and 97.5% empirical quantiles) for seven parameters of the ETAS model, obtained for the 40 Monte Carlo simulations, and the mean length of these intervals for each parameter.

	A	c	α	p	D	q	γ
1	0.0548	0.0211	0.4836	0.3137	0.1128	39.1872	0.5180
2	0.1259	0.0299	0.4526	0.3228	0.0172	5.0844	0.3274
3	0.1358	0.0201	0.4816	0.2922	0.0022	1.0256	0.7182
4	0.1429	0.0161	0.4761	0.3079	0.0135	3.4667	0.5208
5	0.1195	0.0374	0.6282	0.5210	0.0235	9.8750	0.4548
6	0.1170	0.0168	0.4658	0.3014	0.0943	42.6481	0.6373
7	0.1125	0.0257	0.4145	0.2988	0.0655	18.9656	0.2939
8	0.1075	0.0162	0.5065	0.4122	0.0167	7.1181	0.8362
9	0.1112	0.0251	0.4512	0.3713	0.0112	4.7898	0.7041
10	0.1346	0.0301	0.5452	0.3778	0.0724	25.4620	0.3592

	A	c	α	p	D	q	γ
11	0.1232	0.0336	0.4346	0.3052	0.0055	1.3517	0.5010
12	0.1027	0.0380	0.5530	0.5158	0.0809	18.6251	0.4776
13	0.1307	0.0242	0.4840	0.3222	0.0169	5.8331	0.5601
14	0.1181	0.0129	0.4897	0.2656	0.0578	22.2254	0.5660
15	0.1247	0.0232	0.4154	0.2699	0.0066	1.9060	0.4186
16	0.1265	0.0318	0.472	0.3431	0.0065	2.0274	0.3814
17	0.1261	0.0168	0.5494	0.3138	0.0098	4.0845	0.7601
18	0.1342	0.0200	0.5545	0.3083	0.0188	6.4915	0.5328
19	0.1361	0.0210	0.5192	0.3185	0.0077	2.7584	0.6889
20	0.1232	0.0094	0.4818	0.3315	0.0082	3.3808	0.7682
21	0.1497	0.0158	0.6119	0.3352	0.0164	7.4731	0.9777
22	0.1619	0.0125	0.5952	0.2731	0.0238	6.3125	0.4518
23	0.1208	0.0132	0.4784	0.3046	0.0105	2.9628	0.5930
24	0.1273	0.0224	0.4370	0.3533	0.0073	1.9880	0.5798
25	0.1219	0.0155	0.4821	0.3384	0.0145	6.4311	0.7292
26	0.1138	0.0231	0.4526	0.4016	0.0059	2.1749	0.7015
27	0.1419	0.0135	0.6160	0.3510	0.0070	2.2481	0.6093
28	0.1329	0.0182	0.4997	0.3019	0.0128	6.7667	0.8397
29	0.1246	0.0106	0.4478	0.2449	0.0140	3.1429	0.4245
30	0.1271	0.0372	0.4527	0.3752	0.0042	1.8057	0.5709
31	0.1449	0.0278	0.5861	0.3581	0.0076	3.5413	0.7079
32	0.1386	0.0181	0.4886	0.2727	0.0039	1.3773	0.7277
33	0.1294	0.0153	0.4894	0.2884	0.0036	1.2803	0.6852
34	0.1321	0.0164	0.4517	0.2657	0.0124	4.1034	0.4181
35	0.1217	0.0190	0.5281	0.3125	0.0097	2.3168	0.4371
36	0.1596	0.0103	0.5372	0.2322	0.0497	10.4965	0.4788
37	0.1124	0.0286	0.4845	0.3782	0.0117	3.8683	0.3358

	A	c	α	p	D	q	γ
38	0.1214	0.0165	0.5143	0.3069	0.0114	3.4700	0.8259
39	0.1342	0.0125	0.5000	0.2801	0.0250	8.1648	0.3337
40	0.1405	0.0280	0.5521	0.3482	0.0107	2.6838	0.5027
Mean	0.1266	0.0211	0.5016	0.3284	0.0228	7.7229	0.5739